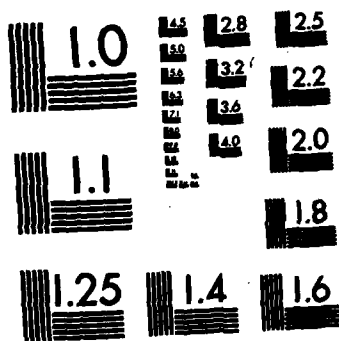END

FILMED

DTIC

MICROCOPY RESOLUTION TEST CHART

NATIONAL BUREAU OF STANDARDS-1963-A

TEMPERATURE AND PARTICLE SIZE DEPENDENCE OF SODIUM
BICARBONATE INHIBITION OF METHANE/AIR FLAMES

Hyung T. Kim

The Pennsylvania State University
Intercollege Research Programs and Facilities
APPLIED RESEARCH LABORATORY
Post Office Box 30
State College, PA 16801

DTIC
S ELECTE D
MAR 2 1983

D

NAVY DEPARTMENT

NAVAL SEA SYSTEMS COMMAND

83 02 023 162

SECURITY CLASSIFICATION OF THIS PAGE *(When Data Entered)*

REPORT DOCUMENTATION PAGE	READ INSTRUCTIONS BEFORE COMPLETING FORM

1. REPORT NUMBER 82-235	2. GOVT ACCESSION NO. AD-A125 105	3. RECIPIENT'S CATALOG NUMBER

4. TITLE *(and Subtitle)* TEMPERATURE AND PARTICLE SIZE DEPENDENCE OF SODIUM BICARBONATE INHIBITION OF METHANE/AIR FLAMES	5. TYPE OF REPORT & PERIOD COVERED M.S. Thesis, March 1983
	6. PERFORMING ORG. REPORT NUMBER 82-235

7. AUTHOR(s) Hyung T. Kim	8. CONTRACT OR GRANT NUMBER(s) N00024-79-C-6043

9. PERFORMING ORGANIZATION NAME AND ADDRESS The Pennsylvania State University Applied Research Laboratory, P.O. Box 30 State College, PA 16801	10. PROGRAM ELEMENT, PROJECT, TASK AREA & WORK UNIT NUMBERS

11. CONTROLLING OFFICE NAME AND ADDRESS Naval Sea Systems Command Department of the Navy Washington, DC 20362	12. REPORT DATE November 3, 1982
	13. NUMBER OF PAGES 88 pp.

14. MONITORING AGENCY NAME & ADDRESS*(if different from Controlling Office)*	15. SECURITY CLASS. *(of this report)* Unclassified, Unlimited
	15a. DECLASSIFICATION/DOWNGRADING SCHEDULE

16. DISTRIBUTION STATEMENT *(of this Report)*

Approved for public release, distribution unlimited, per NSSC (Naval Sea Systems Command), 17 December 1982.

17. DISTRIBUTION STATEMENT *(of the abstract entered in Block 20, if different from Report)*

18. SUPPLEMENTARY NOTES

19. KEY WORDS *(Continue on reverse side if necessary and identify by block number)*

fire, flame, suppression

20. ABSTRACT *(Continue on reverse side if necessary and identify by block number)*

Coal mining/handling operations, as well as those of other powder-using industries, are occasionally interrupted by explosions and fires as a consequence of uncontrolled, fugitive flammable dusts. Damage to life and loss of capital are the unsatisfactory results. Hence, the development of powerful fire extinguishing/suppressing agents to stop these holocausts has become an increasingly important scientific challenge in today's energy and safety conscious world.

The action of the most effective fire extinguishants, which are usually

DD FORM 1473 1 JAN 73 EDITION OF 1 NOV 65 IS OBSOLETE

SECURITY CLASSIFICATION OF THIS PAGE *(When Data Entered)*

alkali metal salts, is still subject to controversy as to whether it occurs via a heterogeneous mechanism (surface catalytic recombination of active species) or a homogeneous gas-phase mechanism (particle evaporation followed by radical capture). Furthermore, the order of effectiveness of various extinguishing agents as determined in laboratory flat flames to date has not matched that as evaluated in real coal dust explosions. Temperature effects have been proposed to explain the last discrepancy.

To resolve such controversies, a special particle delivery system was designed and constructed for the purpose of reliably delivering stable particle concentrations to a quenched flat flame. An investigation was then undertaken on the effect of $NaHCO_3$ particles. This rather innovative approach has indeed generated singular inhibitor effectiveness data that fully explain any previous ambiguities in the flame suppression mechanism of dry chemicals. Moreover, the results of this study can be valuably used to better match effective flame suppression agents to actual fire situations.

Accession For		
NTIS GRA&I	☒	
DTIC TAB	☐	
Unannounced	☐	
Justification		
By		
Distribution/		
Availability Codes		
Dist	Avail and/or Special	

ABSTRACT

Coal mining/handling operations, as well as those of other powder-using industries, are occasionally interrupted by explosions and fires as a consequence of uncontrolled, fugitive flammable dusts. Damage to life and loss of capital are the unsatisfactory results. Hence, the development of powerful fire extinguishing/suppressing agents to stop these holocausts has become an increasingly important scientific challenge in today's energy and safety conscious world.

The action of the most effective fire extinguishants, which are usually alkali metal salts, is still subject to controversy as to whether it occurs via a heterogeneous mechanism (surface catalytic recombination of active species) or a homogeneous gas-phase mechanism (particle evaporation followed by radical capture). Furthermore, the order of effectiveness of various extinguishing agents as determined in laboratory flat flames to date has not matched that as evaluated in real coal dust explosions. Temperature effects have been proposed to explain the last discrepancy.

To resolve such controversies, a special particle delivery system was designed and constructed for the purpose of reliably delivering stable particle concentrations to a quenched flat flame. An investigation was then undertaken on the effect of $NaHCO_3$ particles. This rather innovative approach has indeed generated singular inhibitor effectiveness data that fully explain any previous ambiguities in the flame suppression mechanism of dry chemicals.

Moreover, the results of this study can be valuably used to better match effective flame suppression agents to actual fire situations.

TABLE OF CONTENTS

LIST OF TABLES

LIST OF FIGURES

LIST OF FIGURES (Continued)

ACKNOWLEDGEMENTS

The author wishes to express his most sincere appreciation to Professor J. J. Reuther for his guidance, invaluable advice, and infinite encouragement, and for the opportunity to design and conduct the investigation reported in this thesis.

CHAPTER 1

INTRODUCTION

1.1 General Introduction

Since man first discovered fire, the nature of fire has been
a main subject of investigation in an attempt to control it and use
it efficiently. Most powder-using industries, such as coal mining,
power station boilers, flour milling, grain elevators, plastic and
synthetic resin manufacturers, etc., have occasionally been con-
fronted with dangerous explosions and fires because of fugitive
flammable dusts. The coal dust explosion hazard has long been
recognized and has been the subject of comprehensive surveys from
an operational point of view.[1-3] Approximately 12,000 American
miners have been killed in coal dust explosion disasters since under-
ground mining was first begun in this country.[4] Moreover, estimates
of annual damage expenses incurred as a result of dust explosions
are tens of millions of dollars or more.[1,4]

The proposed study has specifically focused on the solutions
of some of the problems encountered in coal dust explosion suppres-
sion techniques. In the future, the nation's energy demands will
expand with or without changes in foreign oil imports. Hence, the
nation will be required to increase coal-winning and handling opera-
tions, both underground and on the surface, to meet national energy
demands. As a result, the development of techniques for the suppres-
sion and extinguishment of unwanted coal dust/air explosions has
become an increasingly important scientific challenge in today's

energy-and safety-conscious world. Although some progress has been made in this area,[5-9] the identity of the materials that can effectively act as efficient flame suppression agents in unwanted fires remains unclear.

This study in basic research has been designed to eliminate some of the previous experimental ambiguities that have given rise to this dilemma by employing an innovative approach to the study of coal dust explosion suppression by inorganic powders. In order to evaluate the effectiveness of various fire suppressants and to understand the mechanism by which they operate, investigations were conducted on the influence of variables such as maximum flame temperature and combustion gas composition. Methane/air flames were used in coal dust explosion experiments because they allow the simulation of the time-temperature history of this holocaustic event.[5,6]

In order to dope flames with powdered inhibitors, a fluidized bed feeder system was specially developed. Various inhibited combustion profiles, such as those of temperature, combustion product concentrations, and inhibitor concentrations, were obtained as a function of inhibitor feed rate and particle size. The high-priority information and knowledge gained in this study should help to accelerate the successful development of the technology involving devices that will make coal-winning and handling operations safer and less expensive.

1.2 Review of Previous Studies

The mechanisms of flame inhibition action can be broadly divided into physical and chemical mechanisms. Physical inhibition is

characterized by the large quantities of agent required to extinguish the flame.[10] This mode of inhibition occurs in different ways depending on the type of flame involved. For diffusion flames, if an agent partially isolates the combustible from the supply of oxidant, the flame will be retarded. This is generally known as smothering the flame. For premixed flames, if the addition of an agent results in the cooling of the reaction zone, heat production reactions will be retarded, resulting in a decrease in the overall reaction rate. With less heat produced, the amount of heat transferred back to the unburned gas will also decrease. From thermal flame propagation theory, the overall effect of thermal dilution on an adiabatic premixed flame is a reduction in its burning velocity. This phenomenon is known as the cooling effect by the inhibitor.

In contrast to physical inhibition, chemical inhibition is characterized by the relatively small amounts of agent required to retard the flame.[11] If it were possible to sufficiently retard reactions occurring in the flame, the flame would be extinguished. It is a well-established fact that flame reactions involve free radicals and are chain reactions. To be effective chemical flame inhibitors, agents must either serve to break the chains that create the free radicals or catalyze the rate of recombination of these radicals into stable flame gas molecules. It should be mentioned that while the different inhibiting effects can be separated in principle, the action of a given inhibiting agent does not have to fall exclusively in the realm of one or another of the mechanisms.

Flame inhibition has been the topic of many review papers. Most previous flame inhibition research has been directly focused on screening various chemical substances in order to classify them in terms of their flame inhibiting effectiveness. More important investigations are now being performed in order to decipher the chemical mechanism of inhibition. In the last 10 years, therefore, much has been resolved about the fundamental mechanisms operating in inhibited flames.[10,12]

One of the areas of flame inhibition that is controversial concerns the question of whether the inhibition process by alkali salts occurs via a homogeneous gas phase mechanism [13-17] or by a heterogeneous surface recombination mechanism.[18-24] Iya, et al.,[25] studied methane/air flames inhibited by sodium salts and obtained experimental data that correlated sodium atom concentration with the degree of inhibition, independent of the particle size of the solid inhibitor. McHale[26] studied the suppression of the afterburning plume of a rocket motor by potassium salts and performed an equilibrium calculation that gave evidence in favor of one of the proposed gas-phase mechanisms of chemical inhibition. Both of these studies constitute rather conclusive evidence that the inhibition of flames by inorganic salts proceeds via the homogeneous route. With the acceptance of the homogeneous scheme as the most probable mechanism, experimental evidence documenting the dependence of the degree of inhibition on particle size can be explained in terms of rate of volatilization.

Limited success has been achieved in developing devices that can effectively quench coal dust explosions by the dispersion of

water, inorganic powders, or solutions of these two.[3,5,6,7] Experimental mine explosion tests with dry powder chemicals revealed that widely used solid chemical agents had an altered or reversed order of effectiveness in coal dust explosions compared to that determined in high-temperature gaseous flame studies.[7] In some cases, powdered inhibitors were found to be no more effective than water or halogenated hydrocarbons, both of which had previously been found to be inferior to most solid agents in high-temperature flames.[2,6,8] This phenomenon in the order of inhibition effectiveness was quite surprising, and resulted in the limited success achieved in suppressing mine-scale explosions.[7,9] One explanation for this behavior was based on the evaporation rates of the various solid inorganic chemicals. For this hypotheses to be supported, particle volatilization rate experiments in combustion environments for a wide variety of inorganic materials had to be performed. Acquisition of some of these data was the prime experimental objective of the program reported here.

Two major scientific questions concerning coal dust explosion inhibition research have been controversial: (a) how do coal dust particles ignite?; and (b) how do inorganic powder inhibitors act? Both involve a choice between heterogeneous or homogeneous action. From very recent experiments elsewhere, these controversies seem closer to resolution, with indications that homogeneous action is the dominant process in both questions.[7,25] Other studies have covered the evolution and history of research on coal particle ignition[7,9] and on inorganic powder inhibition action.[13-26]

Research on the effectiveness of inorganic powders as gaseous flame suppressants had previously established the following ranking of decreasing effectiveness (on a weight basis) among the salts of interest: $KHCO_3 \cdot Urea$; $KHCO_3$; KCl; $NaHCO_3$; NH_4Cl; $NaCl$; $NH_4H_2PO_4$; and $CaCO_3$.[13,20,21,27-29] The determined value of superiority in effectiveness between one inorganic powder and the next often amounted to about a factor of 2. All but perhaps the last two, $NH_4H_2PO_4$ and $CaCO_3$, were more effective than the best gaseous agents, CF_3Br and CH_3Br.

The aforementioned ranking was expected, by most researchers, to be obeyed in coal dust/air flames. Quite surprisingly, after actual experiments on coal flames were performed, this was found not to be the case.[7,9,30,31] In fact, since $KHCO_3$ was found to be less effective than $CaCO_3$, the ranking was almost completely reversed.[7] If triggered barrier devices had been charged with $KHCO_3$, they would have been essentially impotent at suppressing coal dust/air explosions.

Immediately, because of the severity of the problem, researchers began to rethink theories concerning the behavior of inorganic powders in flames. A significant breakthrough occurred when the first physicochemical data on an actual coal dust/air explosion became available. Again to the surprise of many, it was discovered that the gas-phase temperature in the coal dust/air explosion did not normally exceed 1500°K.[3] It quickly became evident that this maximum temperature was well below that needed to produce sufficient vapor-phase quantities of inorganic inhibitor components. Indeed, since

the original ranking of effectiveness was performed in gaseous flames with temperatures greater than 2000°K, most past research on inhibition by inorganic powders was not directly applicable to coal dust/air explosion suppression research. Hence, a need to know inorganic particle evaporation rates at lower temperatures became timely and important. Since the initial ranking of inhibitors indicated that certain powders ($NH_4H_2PO_4$) were relatively ineffective at extinguishing gaseous flames, little research had been conducted on their modes of action and mechanisms of inhibition.[28] Since it has now been found that chemicals such as $NH_4H_2PO_4$ are among the most effective agents at suppressing mine explosions, basic research on them is now justifiable.[7]

An indirect proof that the evaporation hypothesis is valid and that an indication of the probability that quenched flat flame burner studies of inorganic powder inhibition may provide useful data can be illustrated by information from studies at two separate laboratories.[31,32] Smoot and Horton[31] found that $KHCO_3$ and $KHCO_3 \cdot Urea$ were not effective agents in inhibiting rich coal dust/air flames, but were effective in lean coal dust/air flames. Measurements of particle and gas temperatures of coal dust flames revealed that the maximum gas temperature changed from 1500°K to 2000°K when the coal dust/air flames were switched from rich to lean.[32] This behavior illustrates the utility of proposed variable time-temperature history studies on quenched flat flame burners.

To understand the factors that control inhibitor action, one must understand the coal ignition process. Since coal particle

ignition processes are governed by devolatilization rates, selection of inorganic powders should be governed by the possible effect of the agent on these rates. The validity of this point has been overlooked by most researchers to date. Haynes, et al.,[33] found that many inorganic powders catalyzed coal gasification rates and, thereby, increased the production yield of CH_4 and H_2 from the coal. Since the coal dust explosion inhibitory capacity of these agents may be diminished by this property, inorganic powders should be selected for study with this in mind.

1.3 Objective

The proposed experimental approach is unique in that it is designed to provide data useful to the understanding of the suppression of coal dust/air explosions and gas ignitions, simultaneously. These concerted objectives were achieved by exploiting the versatility of the quenched flat flame burner.[34] Whereas the maximum temperature of an unquenched or adiabatic flame is a unique function of the state of the unburned gas, the final temperature of a flame burning on a cooled porous metal burner can, within limits, be fixed independent of the properties of the unburned gas. In this study, the proper selection of fuel/oxidant system and unburned gas velocity permitted this nonadiabatic device to be used to generate variable residence time/temperature histories that essentially simulated the conditions existing in coal mine dust/air explosions.[5,6,9]

The ultimate objective of this study was to provide data important to those who have been attempting to develop triggered barrier

devices capable of quenching coal mine dust/air explosions. These
practical data were generated by conducting laboratory-scale experi-
ments designed to establish measures of effectiveness and mechanisms
for chemical and physical inhibition of laminar, premixed, and non-
adiabatic flames by inorganic powders. An important goal will
eventually be to identify the agent that is most effective at pre-
venting unwanted coal dust/air explosions.

Important for long-term objectives is that data resulting from
this investigation may aid in the development of superior, second-
generation suppressants that may not only possess far greater inhi-
bitory efficiencies but may also exhibit other synergistic effects,
such as the prevention of reignition. This information may permit
the customizing of agents, or mixtures of them, to various explo-
sion/combustion situations. Hence, the objectives are both limited
and universal in scope; the latter quality may make the results
of this study useful to other organizations besides those involved
in coal-winning and handling operations.

CHAPTER 2

EXPERIMENTAL

2.1 Laboratory Coordinates

Since the data taken on the flames were to be represented in
the form of profile, e.g., temperature versus height above the burner,
careful consideration had to be given to relative and absolute posi-
tion measurements. All relative position measurements were taken
with a cathetometer. The reference surface from which all relative
positions were measured was set by cathetometer reading. This zero
point served as the coordinate origin so that the profiles obtained
with different probes at different stationary positions could be
mapped onto a common coordinate system.

All probes, i.e., the thermocouple, the laser beam, and the
quartz microprobe, were fixed in space, as shown in Figure 1.
In order to measure the maximum flame temperature, the burner-head
was raised and lowered. At the maximum-flame-temperature position,
combustion gases were sampled for analysis with a gas chromatograph.
Laser beam attenuations were measured from the top of the burner-head
into the post-flame zone. Each flame position was held constant in
space, with respect to the burner surface, by careful regulation
of the cold gas composition and flow velocity.

Temperature and laser attenuation profiles were taken at 0.5 mm
intervals above the burner surface. Gas analyses were taken only
at the maximum-flame-temperature position. For the purpose of temp-
erature data reproducibility, scans were made by raising and lowering
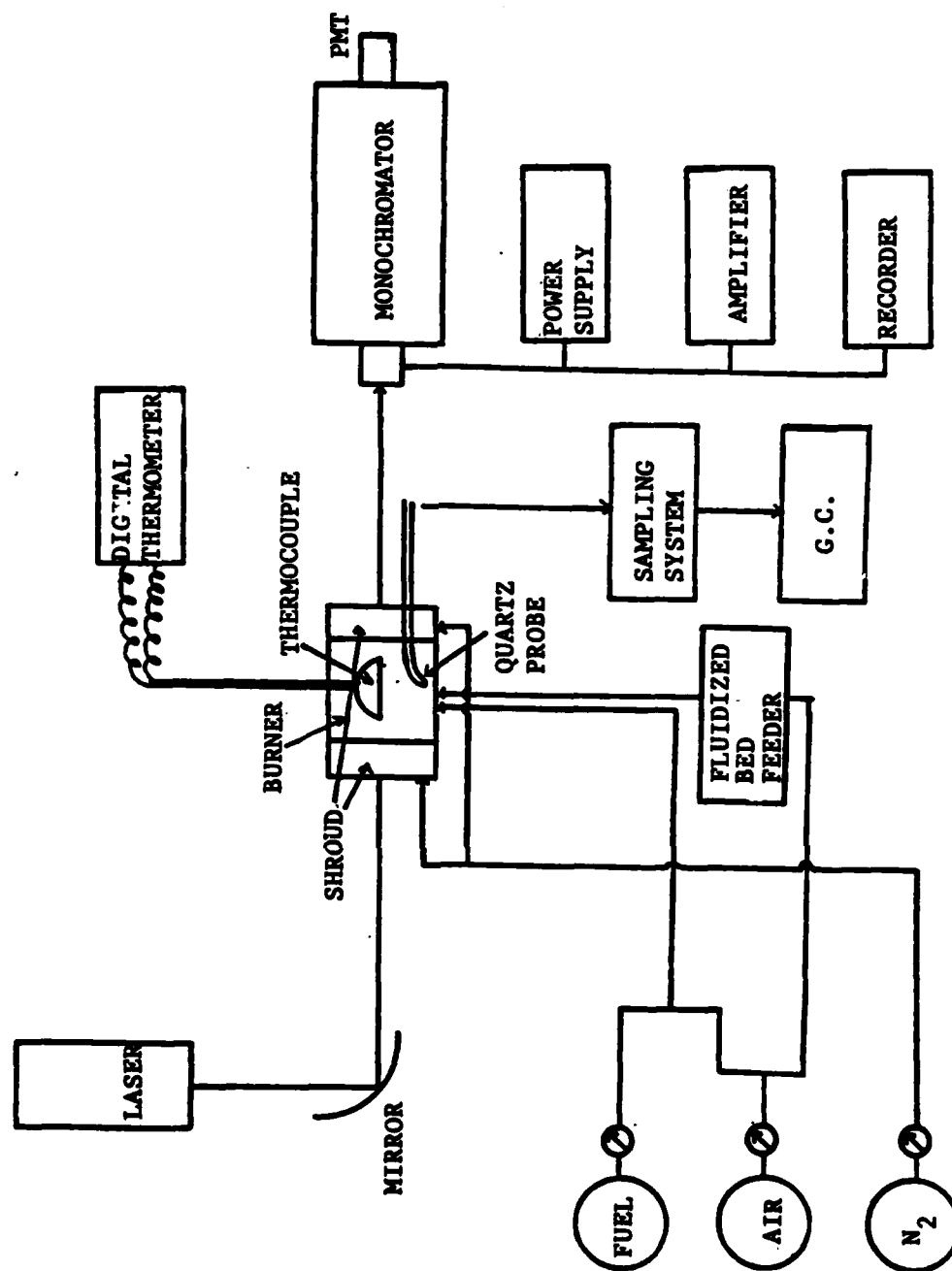
Figure 1. Diagram of the experimental arrangement.

the flame until all levels had been monitored twice. Experiments were conducted with variables based on Table 1.

2.2 Flat Flame Apparatus

Combustion studies ordinarily require a flame of suitable geometry and reproducible stability. A water-cooled, perforated burner, similar to that used by Kaskan and co-workers,[25] was employed in this research. Figure 2 shows two views of the burner. The surface of the burner was a 5 x 5 cm brass plate, 6.35 mm thick, through which were drilled about five hundred 1 mm diameter holes in a regular array. Flames on this burner were continuous sheets, but did display a slight waviness with a periodicity of the hole spacing. The two ends across which the probing beam passed were provided with similarly constructed 5 x 2.5 cm areas. These areas were used for flame shielding in order to prevent the surrounding atmosphere from diffusing into the rectangular flame and causing secondary combustion. Secondary diffusion from the atmosphere could cause any flat flame to distort into a button-shaped configuration. Since some of the flames studied were fuel-rich, the probability of such distortion was of great importance. The nitrogen shroud also performed a second function. If the hot gases from the flame were left unconfined, they would be accelerated upward by the dense surrounding atmosphere, and instead of the post-flame gas zone being a right cylinder hexahedron, it would form into a venturi-like structure. The nitrogen shroud prevented such a distortion.

When a combustible gaseous mixture is forced through a plug of regular array of holes, it emerges as a laminar stream at a

Table 1. Matrix of Experiments

| | Variables | | | | Data Acquisition | | | |
Flame System	Equivalence Ratio ($\emptyset$)	Burning Velocity (cm/sec)	Particle Feed Rate (mg/sec)	Particle Size (microns)	Temperature Profile	POC Profile	Inhibitor Concentration	Inhibitor Evaporation Time
		9	1-10	1-35	x	x	x	x
	0.9	7.5	1-10	1-35	x	x	x	x
		5	1-10	1-35	x	x	x	x
CH_4/Air		10	1-10	1-35	x	x	x	x
	1.1	7	1-10	1-35	x	x	x	x
		5	1-10	1-35	x	x	x	x

Inhibitor: $NaHCO_3$

Pressure: 1 atm for all the experiments

Post Flame Gas Zone

Flame Region

N₂ Shroud

Preheat Zone

N₂ Shroud

Side View:

N₂ H₂O

Fuel/Air H₂O N₂

Top View:

2.5 cm

5 cm

2.5 cm

5 cm
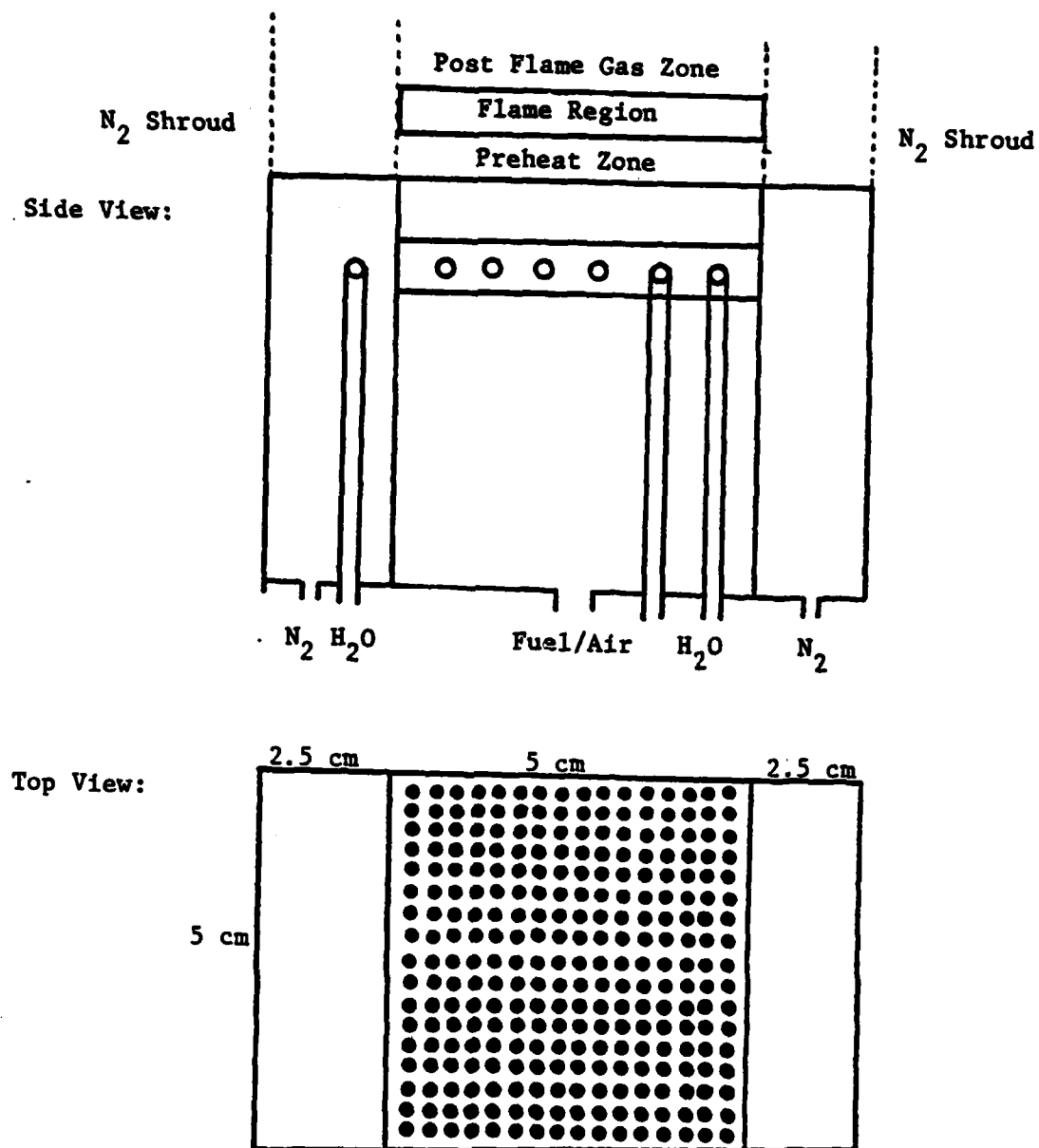
Figure 2. Two views of the flat flame apparatus.

velocity nearly constant over the surface. If the laminar cold velocity of the combustible gas issuing from the plug is less than the normal burning velocity of this composition, then, upon ignition of this stream, a flame will burn through the mixture and stabilize itself as a flat flame, burning in close proximity to the burner surface. In doing so, the flame transfers heat to the burner-head at a rate which is dependent on flow velocity, composition, and pressure.[34] This heat is conducted through the perforated metal to coils, through which cooling water is circulated. Since the cold gas velocity is lower than the normal burning velocity, the actual flame temperature is lower than the adiabatic flame temperature. Thus, with this cooled perforated plug burner, it was possible to vary the flame temperature independent of composition simply by varying the flow velocity.[35] Since the flat flame was stationary at the burner-head, the burning velocity of the flame was equal to the input cold gas velocity.

Precautions were taken to assure that the cooling water was circulating properly at a constant rate during the course of an experiment to prevent melting the burner. The burner was cleaned at regular intervals as there was a tendency for added salt to plug the holes with continued use. The burner was movable in the vertical direction so as to enable data to be taken as a function of vertical distance, and, therefore, time.

2.3 Gases, Burning Velocity, and Gas Regulation

Methane/air flames with varied stoichiometry were employed throughout this experimental research program. In all cases,

compressed cylinder air was the oxidant. Commercially available methane gas (Airco, purity = 99.99%) was used without further purification.

The volume flow rate for a desired burning velocity was calculated from the product of that velocity and the cross-section area (25 cm^2) of the test section of the burner-head. The velocity of the gas issuing from the burner-head was found to be quite uniform over the entire surface area. This was determined by performing thermocouple traverses parallel to the surface of the burner in the presence of a flame. Several of these temperature profiles were taken at different heights above the burner. These maps established that the flames produced by this burner were indeed uniform and flat. Thus, one could probe the flame at any point over the surface and expect equivalent results. Nevertheless, probes were always positioned over the center of the test section where the highest degree of uniformity was achieved.

For quantitative flame studies, one needs to achieve steady-state conditions. Fluctuations of the flame front during the period of measurement should not exceed the required spatial resolution. The usual requirement is ± 0.5 mm over a 10-minute period. Such a steady-state condition was achieved by the use of precise gas regulation.

Gas flows were controlled by a system consisting of a precision gas cylinder regulator in series with a network of pressure gauges and critical flow orifices. The cylinder pressure regulators and the pressure gauges (Nullmatic) were available commercially. The

critical flow orifices were sapphire watch-maker's jewels set in brass

discs, which were held in place by a brass, demountable, orifice

container. The orifices employed had throat diameters ranging from

0.07 to 1.0 mm. The orifice discs were interchangeable in their

containers, so that a range of flow rates could be obtained.

This system had the advantage of great simplicity in providing

known and accurate volume flow rates of gases.[36,37] A critical

flow apparatus consists of a round hole in a plate through which

gas is made to flow. The volume flow through the orifice is inde-

pendent of the downstream pressure and is proportional to the abso-

lute upstream pressure if the pressure ratio across the hole is

greater than the ratio:

$$\frac{P_U}{P_D} > \{\frac{\alpha + 1}{2}\} \left(\frac{\alpha}{\alpha + 1}\right) \qquad (2-1)$$

where: α = specific heat ratio of the gas (dimensionless)

P_U = the upstream pressure (atm)

P_D = the downstream pressure (atm)

This is because the gas passes through the hole at the local sound

velocity and disturbances downstream cannot propagate against the

flow. The volume flow depends on the sound velocity of the gas

in the throat, which is given by:

$$a = (2\alpha R T_U/(\alpha + 1)M)^{\frac{1}{2}} \qquad (2-2)$$

where: a = gas velocity (cm/sec)

R = gas constant (8.314×10^7 erg/mole-°K)

T_U = upstream temperature (°K)

M = molecular weight of the gas (grams)

The volume flow under standard conditions is given by:[38]

$$\overset{\circ}{V}_{STP} = \frac{A\ P_U}{P_D}\ \{\frac{\alpha\ R\ T_U}{M}(\frac{2}{\alpha+1})^{\frac{\alpha+1}{\alpha-1}}\}^{\frac{1}{2}} \qquad (2\text{-}3)$$

where: $\overset{\circ}{V}_{STP}$ = volume flow rate at standard conditions (cm^3/sec)

A = orifice throat area (cm^2)

Thus, one need only have a good upstream gauge to monitor

flow rates accurately. Flow rate was directly proportional to gauge

pressure, without corrections as a result of the fine jewelling

of the orifices.

At a given upstream pressure, the volume of gas flowing through

the tubes to the burner was measured by a wet test meter (Precision

Scientific Co.). The time required to pass a known volume of gas

was measured and from time and volume, flow rate was calculated

and corrected to STP. All the orifices were calibrated with air.

Flow rates for other gases were then calculated by multiplying the

air flow rate by correction factor for each gas. When in opera-

tion, cylinder pressure regulators were kept at a pressure slightly

higher than the required upstream pressure, primarily to assure

a high enough back pressure to achieve critical flow, and secondarily,

to operate economically.

2.4 Temperature Measurements

Temperature profiles can provide valuable information concerning

on the chemical and physical processes occurring inside the flame.

Flame temperature measurements were made by using a silica-coated 2.7×10^{-2} cm diameter, butt-welded Pt/Pt,10%Rh thermocouple.

Despite the existing literature on the subject,[34,39] diffi-culties still remained in the development of techniques required for the construction of a satisfactory thermocouple. Therefore, a short discussion of the method of construction as developed in Professor Reuther's laboratory is recorded so that some details of this art can be preserved.

Thermocouple wires were first threaded through a length of double bore ceramic tubing. With the ends shaped into a Y-form, these leads acted as supports for the actual thermocouple junction and for the electrical leads. The wire components of the thermo-couple itself were first flame-welded to the sides of the support leads. The thermocouple junction was then made by carefully manipulating the side wires, under a microscope, so that the proxi-mity of the ends caused them to be butted. A small capacitor was then discharged through the butt. If this operation were done care-fully, a thermocouple junction weld would form. Butt welding, rather than flame welding, was used in order to obtain the smallest possible bead, which would afford the greatest possible spatial resolution in the flame. With patience and practice, bead diameters of less than twice the wire diameter were obtained. When finished, the wire and bead junction were in the shape of a stirrup. To orient the assembly into a plane, the heavy wire supports were bent so as to put the fine wires in tension.

Initial use of bare Pt/Pt,10%Rh wire thermocouples produced some discrepancies between their measured temperatures and temperatures

obtained by other techniques, e.g., the sodium line reversal method. Friedman attributed this discrepancy to catalytic surface heating from radical recombination reactions on the bare wire.[40] To eliminate or reduce these effects, Leah and Carpenter developed coatings of a ceramic material or fused silica.[41]

To cope with the effects of catalytic heating in this study, fused silica was chosen as the coating material. The silica coating was deposited in the form of a uniform glassy film by immersing the bare thermocouple in the hot gases issuing from a methane/air ($\emptyset = 1.0$) flat flame to which is doped hexamethyl disiloxane (silicone oil). Experience dictated that the best thermocouple coating operation could be done at $1800°K$. At temperatures below $1800°K$, the coating took on a powdery appearance, while at higher temperatures, there was a tendency for the silica to agglomerate into little beads along the wire. These were surface wetting and fluidity problems. To achieve a uniform coating, the entire thermocouple assembly was rotated and moved back and forth continuously as it was being coated. The coated thermocouple was examined under an optical comparator in order to measure the total coated bead diameter. Typical diameters were 0.03 ± 0.005 cm.

The silica coating was found to be durable up to temperatures of $1850°K$, although higher temperatures could be tolerated if the measurement were made rapidly. The temperature range of interest in this study is $1600-2000°K$; higher temperatures of the experiment usually caused the silica coating to strip off rapidly. Instead of continually recoating the stripped thermocouple, a relationship between coated thermocouple and stripped thermocouple was

developed for the purpose of convenience. Temperature measurements were made on stripped thermocouples with a digital thermometer (Omega Engineering, Inc.).

A thermocouple wire glows when it is inserted into a flame. Assuming that the thermocouple wire reaches a steady state with its surroundings, it can be said that the heat gained by conduction is equal to the heat lost by radiation. For heat to be transferred to the thermocouple (in order for the wire to radiate energy), the temperature of the flame gases surrounding the thermocouple must be greater than that of the thermocouple wire itself. This situation illustrates the Zeroth Law of Thermodynamics. This difference in temperature arises because of radiation loss. Correction for this loss was made by equating the heat transferred to the thermocouple by the flame gases to the radiant heat loss from the thermocouple. Note that flame temperature has been subject to many interpretations.[39,42] Radiation loss is the most important correction that has to be made in order to get an accurate measurement of the true flame temperature.

The formulation of the heat balance equation was originally made by Kaskan.[34] In the development of equations describing the physical situation, heat transfer to the thermocouple was best represented by consideration of convective heat transfer because of gas flow at right angles to the axial component of a cylinder. The approach used to derive the necessary equations was based on an empirical correlation between a dimensionless parameter of aerodynamics, the Reynolds number, and the dimensionless parameter of

heat transfer, the Nusselt number. These parameters are defined
as follows:

$$Re = \frac{D \ (\rho v)}{\eta} \qquad (2-4)$$

where: Re = Reynolds number (dimensionless)

D = wire diameter (cm)

ρ = gas density (g/cm^3)

v = velocity of gas (cm/sec)

η = fluid viscosity at the wire temperature (g/cm-sec)

$$Nu = \frac{hD}{\lambda} \qquad (2-5)$$

where: Nu = Nusselt number (dimensionless)

h = heat transfer coefficient (cal/cm^2-sec-°K)

λ = thermal conductivity of the gas at the wire tempera-
ture (cal/cm-sec-°K)

The empirical correlation between Re and Nu for a cylinder in a non-
stationary gas is as follows:[43]

$$Nu = 0.8 \ (Re)^{0.25} \qquad (2-6)$$

Because of the paucity of data in the regions of interest for these
experiments, the absolute numerical values for Nu and Re were obtained
by a linear extrapolation of the log Re versus log Nu curve given by
McAdams,[43] to the low Re values required.

The overall heat balance equation for a unit length of cylinder
was then given by:

$$h\Delta T_{RAD} = \varepsilon\sigma Tw^4 \qquad (2\text{-}7)$$

where: Tw = wire temperature (°K)

ΔT_{RAD} = temperature difference due to radiation loss (°K)

ε = emissivity of the coated thermocouple (ergs/cm^2-sec-°K)

σ = Stefen-Boltzmann constant (1.37×10^{-12} cal/cm^2-sec-°K^4)

From Equations 2-6 and 2-7, the equation for the temperature correction because of radiation loss can be derived. It has the following form:

$$\Delta T_{RAD} = \frac{1.25 \ \varepsilon\sigma D^{0.75} \ Tw^4}{\lambda}(\frac{\eta}{\rho v})^{0.25} \qquad (2\text{-}8)$$

In the application of Equation 2-8, gas thermal conductivity, viscosity, and density were appropriate to a high temperature, multi-component flame gas mixture. The values of these transport properties for various gases, used in the calculation of true temperature, were investigated by Hilsenrath, et al.[44] The diameter of the coated thermocouple was determined microscopically to be ca. 2.7×10^{-2} cm. The numerical value for the emissivity was determined by Kaskan to be 0.22 at 1600°K.[34] This value was used exclusively in this work, and its temperature dependence was neglected.[45]

The true flame gas temperature, T_F, was then calculated using a microcomputer. First, thermal conductivity, viscosity and density were catalogued for each flame temperature. The temperature difference because of radiation loss was calculated using Equation 2-8; and the final flame temperature was then calculated from the following:

$$T_F = T_w + \Delta T_{RAD} \qquad (2\text{-}9)$$

Typically, the radiation loss correction was in the range of 50-150°K.

2.5 Particle Delivery System

A singular fluidized bed feeder was developed to provide a stable flow of fine particles to the flat flame burner. Advantages associated with a fluidized feeder technique are the inexpensiveness of construction, the straightforwardness of fabrication, the wide range of stable particle flows, the simplicity of operation, and the reproducibility of results.[46] However, it can often be plagued by plugging problems which can be avoided by pulse feeding or by predetermining the particle flow rate.

The details of the fluidized feeder are illustrated in Figure 3. First, pulverized particles were poured into the cylindrical glass feeder housing through the top assembly which was clamped to the housing. The particles rested at the bottom of the housing on a fritted glass disk filter. Fluidizing gas entered at the base of the glass housing and passed upward through the fritted disk filter. In operation, the lower portion of the bed exhibited a dense fluidized state. A lower-density, spouted-bed region of particles was obtained by passing a secondary flow of the carrier gas through a small venturi in the lower portion of the bed. The venturi was formed by a hole that was drilled in the side section of 1 mm bore capillary. This capillary tubing was connected to the secondary carrier gas tubing. Particles from the dense fluidized bed were
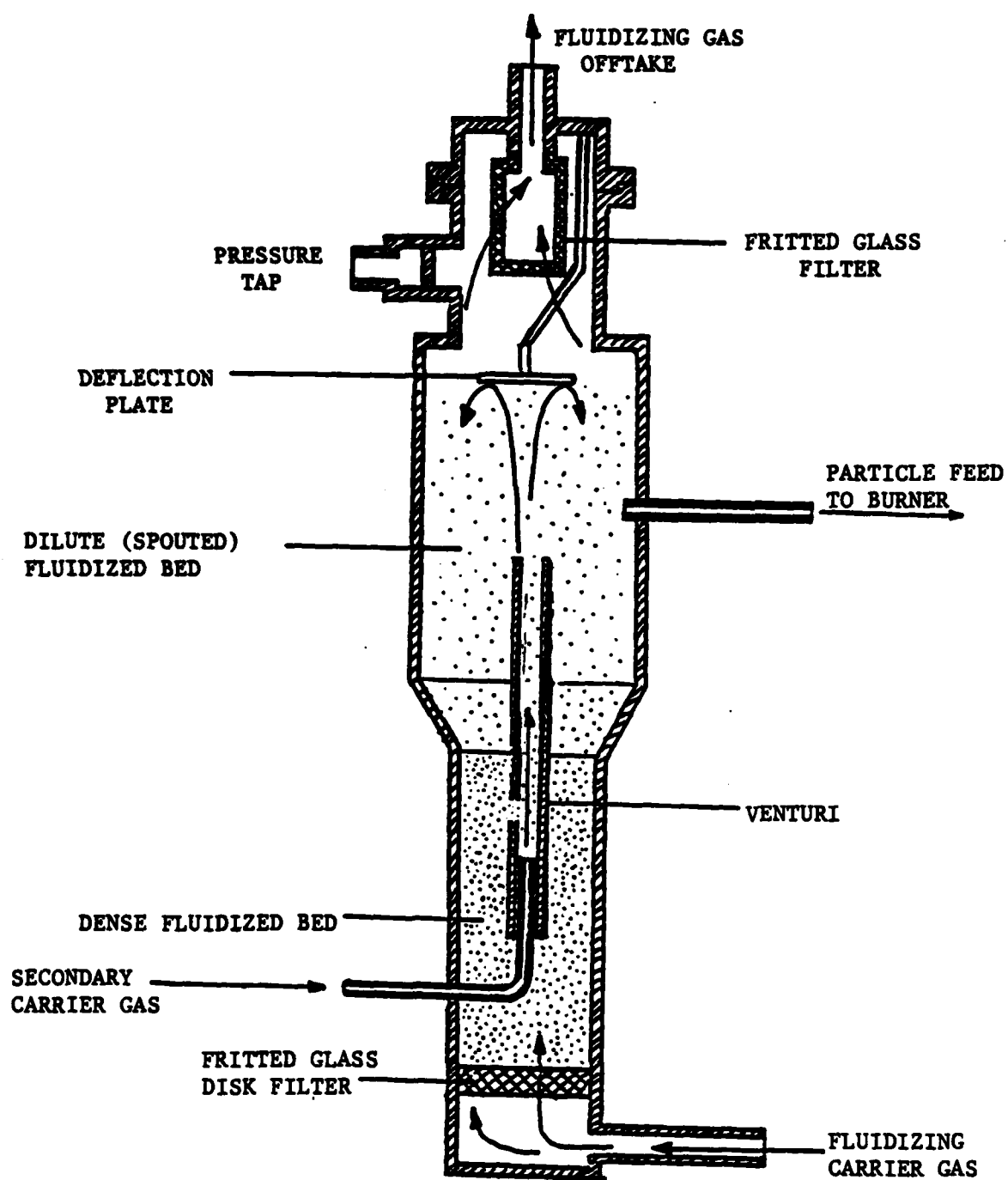
Figure 3. Schematic of the fluidized bed feeder.

entrained in the capillary tubing by secondary flow and impinged on the glass deflection plate suspended from the top assembly. The entrained sample particles formed a low density, spouted particle shower that returned to the dense bed. Flexible stainless steel tubing was positioned within the low density particle shower to permit the transport of particles to the reactor by virtue of the pressure drop between the fluidized feeder and the atmospheric pressure of the reactor.[47]

The mass flow rate was measured by suspending the entire fluidized bed assembly from a precision balance (Mettler PC440) and noting the weight loss per unit time. The entire fluidized feeder was calibrated according to the mass flow rate of particles as a function of pressure, measured by a manometer that was attached to the housing. Because of the high sensitivity of the system, the entire fluidized feeder assembly was enclosed in a Plexiglas box in order to eliminate drafts.

Feeding particles in the burner first required the fluidization of the particles in the bed. Assume that a fluid passes upward through a fixed bed of particles. When the frictional drag on the particles becomes equal to their apparent weight (actual weight less buoyancy), the particles become rearranged so that they offer less resistance to the flow of fluid and the bed begins to expand.[48] This process continues as the velocity is increased until the bed has assumed the loosest stable form of packing. In this process, the total frictional force remains equal to the weight of particles. Further increase in the fluid velocity separates individual particles

from one another and particles become freely supported in the fluid.[49]

This phenomenon is called fluidization. Increased fluidization

velocity causes the particles to separate still further from one

another.

After fluidization, the particles were transported by entrain-

ment from the fluidized feeder into the reactor through the small

bore stainless steel tubing. In the experimental condition of small

cross section of transport tubing, the fluid velocity was so fast

that it was logical to express the particle velocity as the fluid

velocity for the entire length of transport line under consideration.

Within this assumption, the mass flow rate was calculated from the

following:

$$\dot{m} = A \, \rho_t \, U \qquad (2\text{-}10)$$

where $\dot{m}$ = mass flow rate (g/sec)

A = cross-section of transport tubing (cm^2)

ρ_t = total density (g/cm^3)

U = fluid velocity (cm/sec)

The total density, ρ_t, was obtained from a solid holdup experiment,[50]

by dividing the weight of the solid collected by the total volume of

the gas-particle flow.

Apparently, the mass flow rate was roughly proportional to

fluidizing velocity provided that total density was constant in

the range of all transport line. Furthermore, the fluid velocity

had the following relationship to the pressure difference[49]:

$$\Delta p \propto U^2 \qquad (2\text{-}11)$$

where: Δp = pressure difference between inside the feeder and atmosphere (Hg cm)

For fluidized feeder calibration, the pressure difference across the fluidized feeder was used as a criterion for measuring the mass flow rate. The governing equation is[49]:

$$\dot{m} \propto A\rho_t \sqrt{\Delta p} \qquad (2-12)$$

The pressure drop was measured by a mercury manometer, attached to the fluidized feeder housing, was used to find the value of mass flow rate on the calibration curve.

Sodium bicarbonate was employed as the inhibitor powder and was CP reagent grade. It was milled in a ball mill to reduce the average particle size and was then treated, i.e., siliconized by the use of Dow Corning 1107 Fluid, to improve dispersability. Samples of each grind were classified into three fractions of different average particle size. Table 2 gives the characteristics of the fractions employed, including nominal diameter range, diameters between which 90% by weight of the particles fell, and surface area per gram. The areas were calculated by assuming the particles to be spherical and determining the sum[25]:

$$A_s = (6/\rho) \sum_{i=1}^{10} (W_i/d_i) \qquad (2-13)$$

where: A_s = surface area per gram

d_i = average diameter of ith fraction

W_i = weight fraction of ith fraction

ρ = particle density.

Table 2. Characteristics of the NaHCO$_3$ fractions employed.

Nominal Size, μ (microns)	Diameter Range Containing 90% by Weight, μ (microns)	Surface Area (cm^2/g)
0-10	3-13	4886
10-20	12-38	1562
20-35	16-47	1086

In the initial attempts to siliconize the sodium bicarbonate, it was found that the powder was being converted to sodium carbonate (Na_2CO_3). For the samples actually employed, care was taken to prevent this, and the fact that the product was still mainly $NaHCO_3$ was verified by analysis of the product.

2.6 Combustion Gas Concentration Measurements

One of the objectives of this study was to analyze stable flame species for the purpose of understanding how they were changed upon inhibition. In this investigation, the sampling process did not destroy the species of interest. Although this statement seems to indicate that hydrocarbon probe sampling is a straightforward process, the original application of this technique in flame analysis gave some problems.[51] The experimental method turned out to be simple in concept but complex in execution. The determination of composition profiles by probe sampling involved a number of conflicting experimental requirements, which required a compromise. For the hydrocarbon/air flame system, technical problems were solved by the use of small quartz microprobes for sample withdrawal, followed by flame gas analysis by a gas chromatograph.

The sampling probe was a water-cooled, quartz microprobe, contoured from 5 mm quartz tubing drawn down to a capillary tip. The taper of this tip extended over 2 cm and subtended an angle of 5°. The orifice was 0.5 mm in diameter and its tip was ground flat and flame-polished. This particular probe had been previously designed, built, tested, and successfully employed.[52] Since the use of this probe had a critical bearing on the outcome of the experimental

results, an investigation was made into the thinking behind the
design and fabrication of the probe, along with the precautions that
had to be exercised in the interpretation of the data.

The probe had to withstand temperatures as high as those
found in flames, which are generally around 2000°K. Although
quartz has a softening temperature of 2000°K, it has been successfully
used in flames at more than 2000°K, since the quartz itself is cooled
through radiation loss.[53] With thermocouple measurements indicating
that flames were at 1600-2000°K, quartz was quite safely acceptable
as a probe material.

The probe had to have specific overall dimensions so that its
presence did not appreciably disturb the laminar streamlines of
the flame. Insertion of an object into a flame causes bulk intrusion
effects, which have been theoretically treated by Tine.[54] From
the book of Tine, it was shown that the specifications of the probe
available in this lab would not cause great aerodynamic disturbances
to the flame front. Recent studies have shown that the 5° probe
angle has minimal influence on the flow field.[55]

The probe was oriented perpendicularly over the center region
of the burner, where the temperature mapping was most uniform. Bulk
disturbances by the probe were further minimized by introducing
it from the downstream side of the post-flame gas zone. Visual
observations could not detect any distortions to the flame. The
appearance of the probe in the flame was similar to a photograph
taken by Fristrom, et al.[56]

Not only were bulk, aerodynamic disturbances taken into account,
but so were possible chemical disturbances. Quartz is nonreactive

in flame gases if its surface is clean. To reduce any catalytic effects of the probe, i.e., its ability to catalyze radical recombination on its surface, the quartz probe was cleaned by treatment in hot concentrated nitric acid, followed by a thorough distilled-water rinse, followed by oven drying. Any catalytic activity on the probe surface would be revealed by bright spots on the probes; no bright spots were observed.

When a probe is used to withdraw a few micrograms of sample from hot flame gases, one would like to have all chemical reactions rapidly quenched at the point in the flame where the probe orifice is located. This assures that the probe will transfer a sample that is reliably representative of an instant of time corresponding to distance along the axial flame axis. Chemical reactions were immediately quenched upon entry into the probe by rapid decompression (large pressure drop) and immediate withdrawal of the sample into a cooler region (large temperature drop). The former process was accomplished by taper design, orifice diameter, and pumping speed, while the latter was accomplished by water-cooling in and behind the probe head.

The probe tip and withdrawal channel were mated to a sampling system consisting primarily of a standard vacuum rack. A back-pressure of 7×10^{-5} atm was maintained in this system with a mechanical pump (Duoseal 1400). Pressure in the rack was monitored by a thermocouple gauge (Veeco, TG-70). Batch samples were collected in 50 ml bulbs.

It was important to examine the experimental conditions used to collect flame gas samples in order to assure that rapid adiabatic

expansion and quenching were achieved. Rapid quenching was the most important consideration. Since the half-lives of most chemical reactions in flames are of the order of 50 microseconds, the quenching process must be exceedingly rapid.[51] Such quenching can only be achieved when the experimental conditions and the probe specifications satisfy the requirements for flow through the probe.

Initially, the probe orifices were chosen so as to be the smallest that would still yield a reasonable flow rate. Small probes also diminish flame distortion. However, sampling rate decreases gradually with orifice diameter. Therefore, by going to small probe diameters, quenching rates were slowed down. Furthermore, critical flow is dependent on the mean free path being small compared to the orifice diameter. As probe inlets become smaller, this requirement becomes less satisfied. The trade-off between these mutually contradicting requirements was ameliorated by the effect of pressure on sampling. Sampling rates increase as pressure in the sampling rack decreases.

Another important experimental condition considered was the need for a large pressure drop across the orifice to assure isentropic expansion of the bulk fluid in the probe. For a burner chamber pressure of 1 atmosphere and a probe back-pressure of 7×10^{-5} atm, calculation of the aerodynamics of the probe indicated that all the chemical reactions were successfully quenched.[56]

The sampling system and the sample bulbs were pumped down to below 7×10^{-5} atm. The sampling system and bulbs were then isolated from the pump and the sampling system was opened to the probe and to the flame. When sampling commenced, the probe

tip was seen to glow brightly and uniformly, more so than with no sampling. It should be noted that radiation loss and heat sink effects were accounted for and had been shown to be negligible.[51] The glowing was the result of the introduction of hot gases into the probe and their quenching. It was assumed that sufficient sampling had been accomplished after two minutes. At this time, the sample bulb and the probe were isolated from the sampling system and the system was evacuated. Sampling bulbs were flushed out with the flame gas just sampled for the purpose of conditioning. This procedure was practiced so that it could be performed quickly and accurately, since expensive high purity gases were being consumed during the process. There was no pumping behind the probe when it was open to the sample bulb. In separate experiments, such pumping was observed to cause visible disturbance to the flame, i.e., flame puckering and attachment to the probe. Also, back pumping cooled the downstream gases. This cooling was observed as a dark spot in the flame reaction zone.

Gas chromatography offers a versatile and reliable experimental technique for obtaining analyses of flame gases. It was by this technique that the composition profiles of the major species in flame were determined. The analytical gas chromatography (Carle-s-157A) produced spectra with peaks representing concentration with respect to retention times for each species. Combustion species with different thermal conductivity values enabled the display of these peaks as a function of retention time.[57]

The gas chromatograph was calibrated with standard sample gases (Scott Environmental Technology, Inc.). Carbon dioxide, carbon

monoxide, methane, hydrogen, oxygen, and nitrogen concentrations were standardized via calibration. Water concentrations were calculated from oxygen and hydrogen atom balances.

In the process of sampling combustion gases, ambient air might be introduced into the sampling valve of the gas chromatograph, so that the oxygen concentrations are increased by a measurable amount. Furthermore, some oxygen-containing compounds, such as alcohols, aldehydes, and acids, might be formed in the combustion process and as such, would tie up oxygen in a form other than H_2O and CO_2. Because of these possibilities, water concentrations were first determined based on a hydrogen-atom balance, which, for obvious reasons, is more accurate than that based on an oxygen-atom balance. The total carbon atom number is the sum of the concentrations of all carbon-containing species:

$$\text{Total C} = [CO_2] + [CO] + [CH_4] \qquad (2\text{-}14)$$

where: Total C = total carbon atom number

$[CO_2]$ = carbon dioxide concentration

$[CO]$ = carbon monoxide concentration

$[CH_4]$ = methane concentration

Water concentrations were then calculated by Equation 2-15, in which the total hydrogen atom number is four times the total carbon atom number, because methane/air flames were used exclusively in this experiment:

$$[H_2O] = \frac{\text{Total H} - 2[H_2] - 4[CH_4]}{2} \qquad (2\text{-}15)$$

where: $[H_2O]$ = water concentration

Total H = total hydrogen atom number

$[H_2]$ = hydrogen concentration.

Chromatographic data on molecular hydrogen concentrations sometimes appeared to devalue the calculated water concentration because of reproducibility difficulties in H_2 detection. In suspect cases, water concentrations were also calculated by an oxygen-atom balance. The total input oxygen atom number was first calculated by the following:

$$Total\ 0 = \frac{[N_2] \times 2}{3.76} \tag{2-16}$$

where: Total 0 = total oxygen atom number in air

$[N_2]$ = nitrogen concentration in air.

Then, product water concentrations were calculated from the following:

$$[H_2O] = Total\ 0 - 2[O_2] - 2[CO_2] - [CO] \tag{2-17}$$

where $[O_2]$ = oxygen concentration.

The water concentration values obtained by these two complementary methods agreed quite well with each other given the experimental error and assumptions in the calculation. Trace species, such as alcohols, aldehydes, or other hydrocarbons, were not a source of error because their concentrations were measured to ca. 0.01 percent. All these calculations were performed using a microcomputer.

2.7 Laser Attenuation Measurements

This technique was used to measure inhibitor particle concen-
trations above the flat flame burner in order to determine particle
evaporation rates. To this end, the attenuated laser beam intensity
was measured as a function of inhibitor particle residence time,
i.e., height above the burner surface.

The reasoning behind these experiments was developed by Wersborg,
et al.[58] The spectral cross-section, C_{abs}, and particle volume con-
centration were calculated from the Lambert-Beer law as follows:

$$I_\lambda = I_{o\lambda} \exp\ (-C_{abs}\ \eta L) \qquad (2\text{-}18)$$

where: I_λ = intensity of attenuated beam

$I_{o\lambda}$ = intensity of original beam

C_{abs} = spectral cross-section

η = particle number concentration

L = path length.

From the plot of intensity, I_λ, versus distance above the burner,
the particle evaporation time was deduced.

A He-Ne laser (HN-2S, Jodon Engineering Associates, Inc.)
was used as a light source in the attenuation experiment. Since
good alignment, position, and focus were important in the optical
probing experiment, this laser also was employed in the optical bench
alignment process. The attenuated laser line, having a wave length
of 6328 Å, was received by scanning monochromator (Spex Industries,

Inc, model 1870), fitted with a photomultiplier tube (EMI Gencom, Inc., 9659 A) and powered by high voltage supplier (Keithley Instruments, model 244). The resulting signal was then refined by a phase-sensitive detector (Keithley Instruments, model 840) and recorded on a strip chart.

2.8 Determination of Experimental Uncertainty and Error

The error or uncertainty in the numerical values obtained in these experiments was difficult to assess because both measured data and a priori data were incorporated into the overall calculations. A detailed analysis of the propagation of error would, therefore, be difficult to perform. If performed, the results would be crude and difficult to interpret.

In place of an elaborate statistical error analysis, consideration was given to: (a) those laboratory parameters which were considered to be known and reliably controlled; (b) reproducibility of data; and (c) comparison of lab data with literature data.

The first laboratory parameter considered was the flow rate. Flow rate controlled the cold gas velocity which controlled the flame speed. In these experiments, flame speed was set constant for each experiment. Critical flow orifice meters were used to control the gas flow velocity. These have been rated to be accurate to ± 0.1%.[37] Day-to-day fluctuation of flow rates was measured at about this value.

The accuracy in determining the relative position of the various probes, upon which the entire general coordinate system relied,

was as good as the cathetometer reading. The cathetometer was built
to be accurate to $\pm$ 0.1 mm. The reproducibility in the effective
positions of the various probes and reference surface was ca. $\pm$
0.5 mm. All levels were scanned with movement translating upward
and downward, and reproducibility was very good. The resolution
of the laser attenuation measurements was limited by the width of
the laser beam, which gave a spatial resolution of 1 mm.

The source of error in temperature was because of the uncer-
tainty in the determination of the emissivity of the quartz-coated
fine-wire thermocouple.[34] Kaskan stated that day-to-day reproduci-
bility of thermocouple readings should be approximately $\pm$ 2.0% in
the temperature range of 1700-2000°K. Actual reproducibility was
typically better than these quotations. All temperature measurements
were taken quickly; the reproducibility of these "instant" recordings
was $\pm$ 5°K. With the thermocouple held at one point in the flame,
negligible temperature fluctuation occurred over a period of 10 minutes.

The error in gas chromatographic analysis of the sampled flame
gases was estimated by comparing unburned fuel/air mixtures prepared
by the critical flow meters with the output response of the gas
chromatograph. Gas chromatographic data were found to be $\pm$ 5% accurate
in the calibration mode. The reproducibility of the analysis of
a gas sample taken from the same height of the same flame in experi-
ments done on different days was found to be $\pm$ 5%.

CHAPTER 3

RESULTS AND DISCUSSION

3.1 Temperature Profiles of Clean, Uninhibited Flames

Measurements of flame temperature as a function of height above
the burner surface were made on methane/air flames with fuel-rich,
stoichiometric, and fuel-lean compositions and with varied cold
gas velocities. Composition was expressed as equivalence ratio,
$\emptyset$, which is the ratio of the actual fuel/air ratio to that of the
stoichiometric proportion. These data are plotted in Figures 4,
5, and 6 in the form of flame temperature versus the vertical height
above the burner surface. The reported temperatures are the thermo-
couple wire temperature corrected (raised) for radiation loss; height
was determined using a cathetometer.

As can be seen from the data in Figures 4, 5, and 6, temp-
eratures were recordable from the pre-flame zone to the post-flame
zone. The temperature first rose steeply in the pre-flame zone
to the leading edge of the reaction zone, reached a maximum at the
end of the reaction zone, and then remained at a near-constant or
slightly decreasing value throughout the post-flame zone.

Since it was the intention to utilize the perturbation of the
clean flame temperature profile as a measure of inhibitor effec-
tiveness, some thought was given as to the nature of the profile
shape. Theoretically-derived temperature profiles were first devel-
oped with thermal theories dating back to those of Mallard and Le
Chatelier.[39] They proposed that it was a propagation of heat back
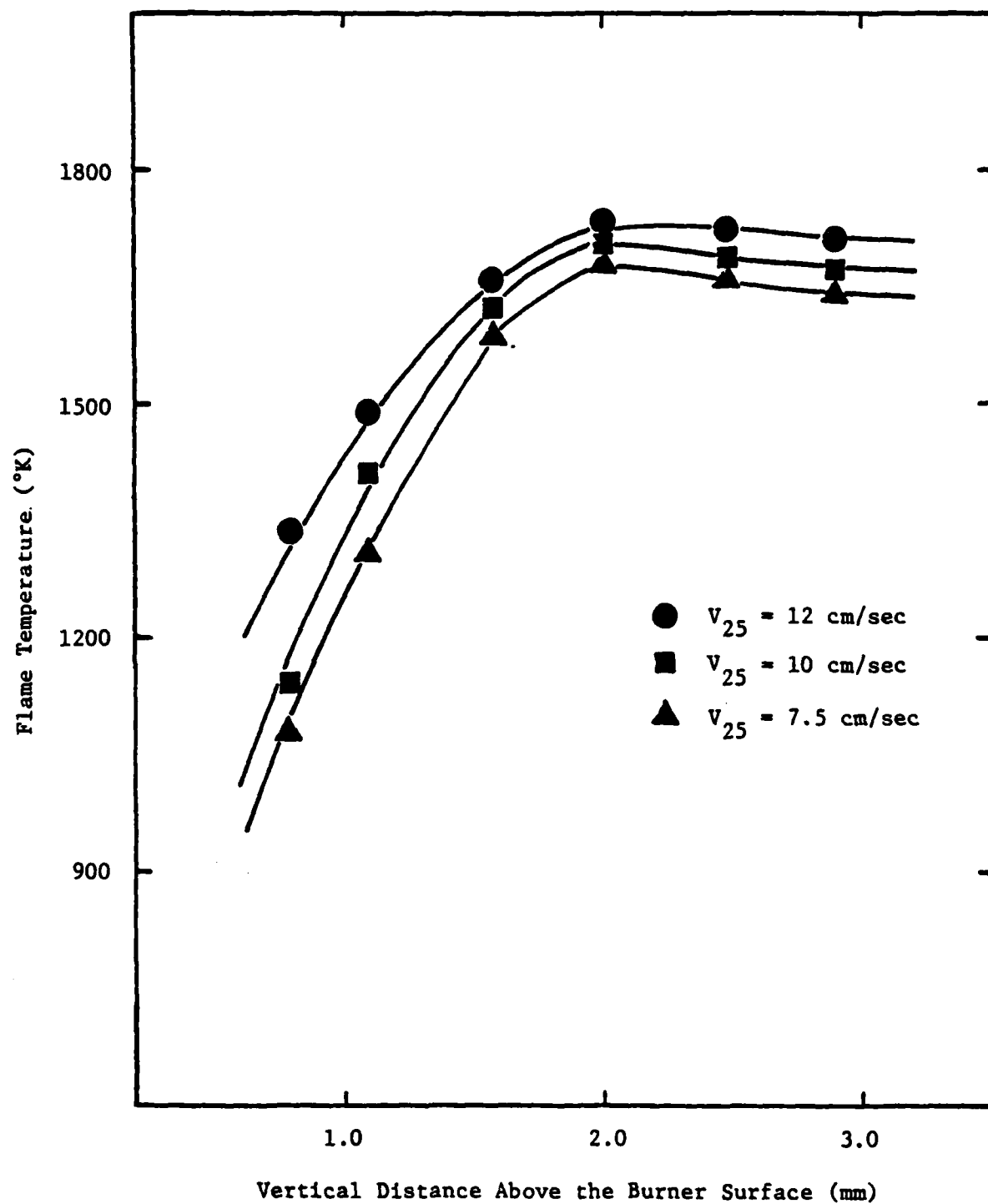
Figure 4. Flame temperatures in a $\emptyset = 0.8$ methane/air flame as a
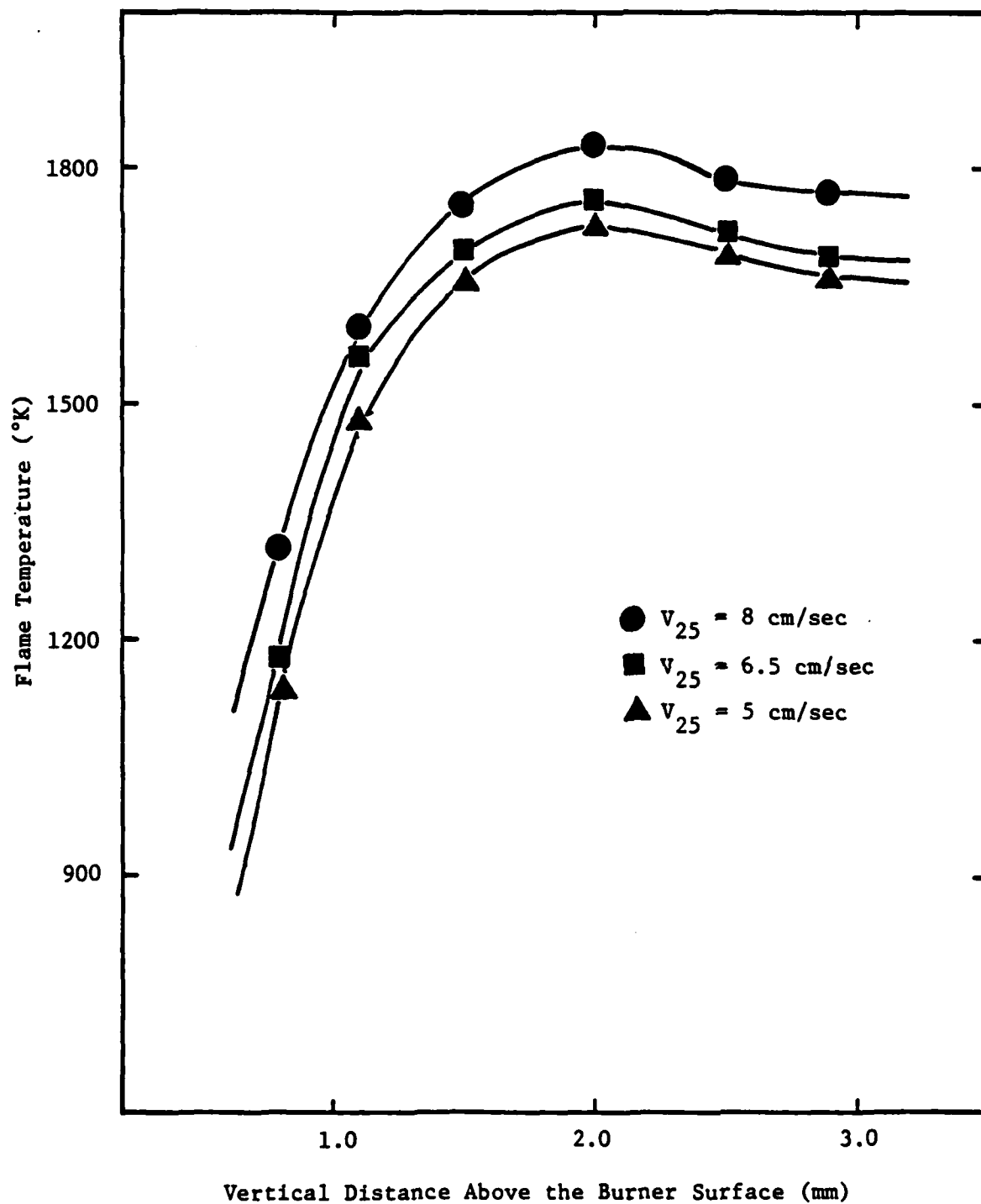function of vertical distance above the burner surface.

Figure 5.   Flame temperatures in a $\emptyset = 1.0$ methane/air flame as a
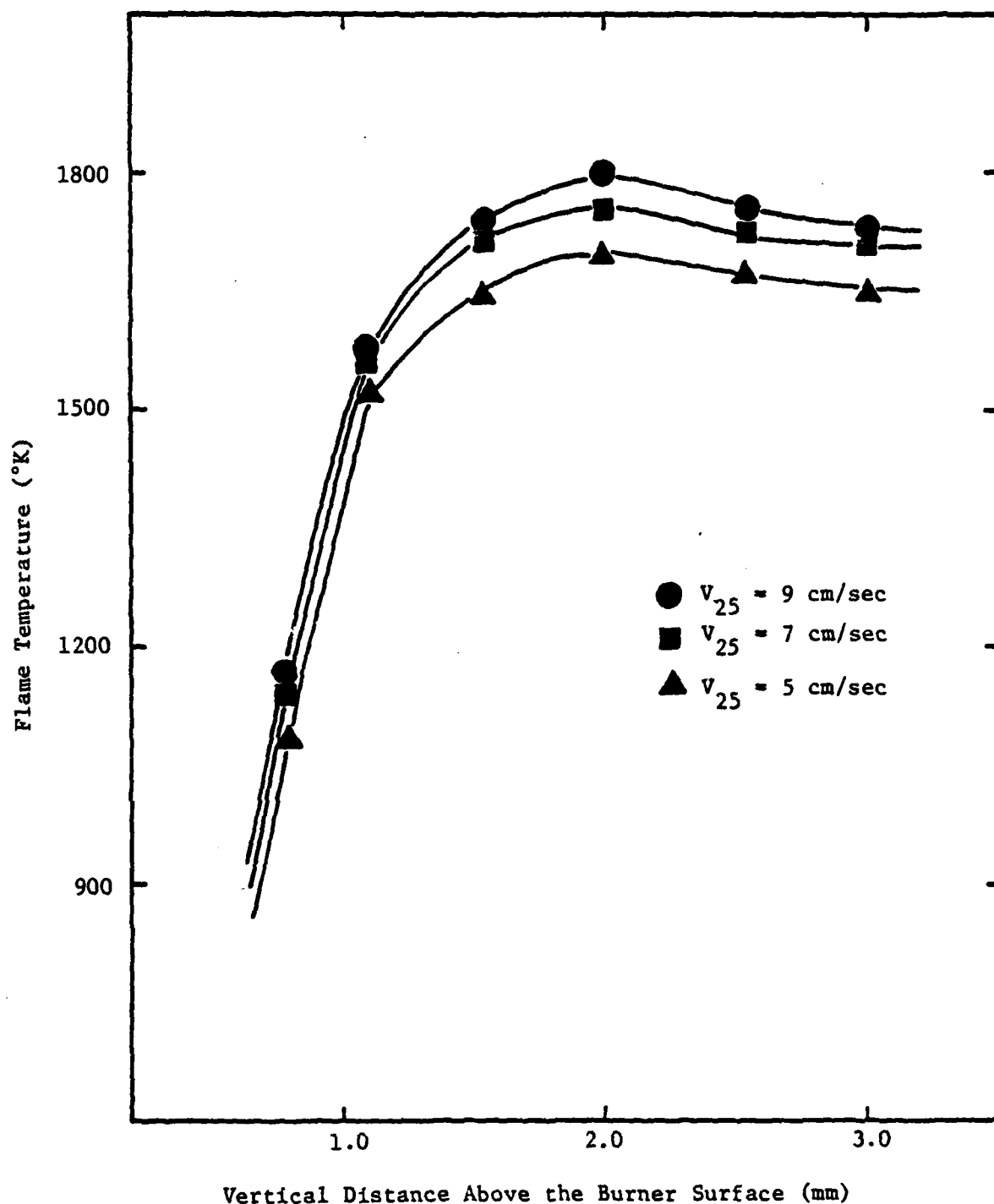function of vertical distance above the burner surface

Figure 6.   Flame temperatures in a $\emptyset$ = 1.2 methane/air flame as a
function of vertical distance above the burner.

through layers of unburned gas that was the controlling mechanism in flame propagation.[59] Unfortunately, the use of this thermal theory requires the concept of a specific ignition temperature, as of yet experimentally ill-defined, and neglects the effect of diffusion of molecules, free radicals, and atoms. Theories for particle diffusion mechanisms were first put forth in 1934 by Von Elbe and Lewis.[60]

A unit mass passing through the combustion wave at first receives more heat by thermal conduction from the hotter downstream elements than it loses to the upstream cooler elements, so that its temperature increases above an initial level. At some higher temperature, the mass element is transformed from a heat sink to a heat source in the sense that it now loses more heat to the upstream elements than it receives from the downstream elements; its temperature continues to increase, owing to chemical heat evolution, until the supply of chemical energy is exhausted. In this process, reaction zone thickness is typically characterized as the region from the point where the heat to the upstream elements equals the heat from down-stream elements to the point where the chemical reaction is completed. With this definition of reaction zone thickness in mind, the thickness of each flame under investigation was determined as being about 1 millimeter, independent of composition and of cold gas velocity. This information was used in calculations of the residence time of particles in the flame front without further refinement.

3.2 Particle Feed Rate Measurements

A mercury manometer was attached to the fluidized feeder housing and a bed pressure drop index was used in the calibration of particle feed rate to the flame. Each particle size range of siliconized $NaHCO_3$ was individually introduced into the fluidized bed feeder for calibration. By the action of primary and secondary carrier gases, particles were suspended inside the feeder and then delivered to the reactor. Calibration of the particle feed rate was carried out by establishing the relationship between the mass feed rate and particle velocity, which was determined by the pressure difference between that inside the fluidized feeder and that of the laboratory, which was atmospheric.

The entire fluidized feeder was suspended from a balance and its rate of weight loss was measured as a function of pressure drop registered by the mercury manometer. The particle feed rate was determined as the quotient of weight loss divided by the time span of the measurement. In Figure 7, plots of the particle feed rate against pressure difference for the three different particle size ranges were used.

Mass flow rate could be theoretically calculated as a product of total density, area of the duct, and particle velocity. Particle velocity is normally proportional to the square root of the pressure drop. As a result of this, the mass flow rate should be proportional to the square root of the pressure difference. For the data in Figure 7, however, the mass flow rate was found to be proportional to the square of the pressure drop. This apparent contradiction was
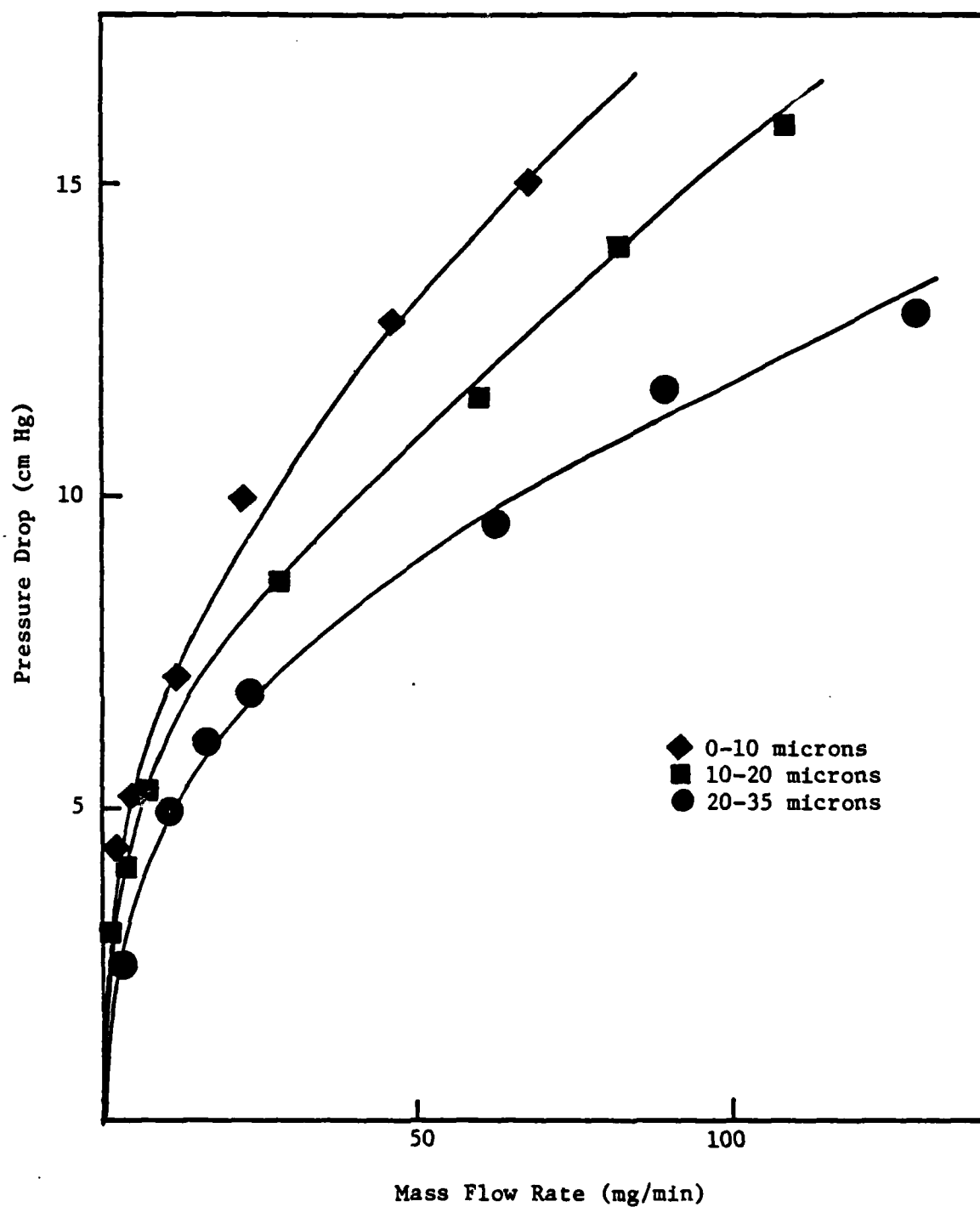
Figure 7. Particle mass flow rate in fluidized bed feeder as a function of pressure drop in mercury manometer.

explainable by intuition and knowledge of the process of par-
ticle distribution fractionation. Upon fluidization, particles
can be distributed fractionally throughout the feeder, i.e., light
particles can have longer residence times in the entrained zone
than heavier ones. At a low mass flow rate (low particle velocity),
only the light fraction of particles will be entrained. The rela-
tionship between the mass flow rate and the pressure drop becomes
related to the square root of particle mass rate ($P \propto \sqrt{\dot{m}}$). At some
higher mass flow rate, this mechanism of particle distribution frac-
tionation can be counter balanced by the square root relationship
of mass flow rate and pressure difference for the entire distribu-
tion, and turned into a linear relationship ($P \propto \dot{m}$). Further increase
in the mass flow rate will cause the square relationship of mass
flow rate and pressure drop to dominate, giving the mass squared
dependent ($P \propto \dot{m}^2$). This explanation of the particle action in the
fluidized feed is borne out by the experimental results illustrated
in Figure 7.

3.3 Particle Residence Time

The flame inhibition study was carried out on methane/air flames
with fuel-rich ($\emptyset = 1.1$) and fuel-lean ($\emptyset = 0.9$) equivalence ratios.
The cold, unburned gas velocity was also varied from 5 to 10 cm/sec.
Reaction zone and preheat zone thickness were routinely measured
to be about 1 mm independent of gas composition and cold gas velocity.
The residence time of a particle in the flame was calculated by
the following equation[39]:

$$t_R = \frac{2d}{V_{25}(T_f/T_o + 1)} \qquad (3-1)$$

where: t_R = residence time

   d = thickness of the preheat zone plus reaction zone

   V_{25} = cold gas velocity

   T_o = ambient temperature

   T_f = flame temperature.

The combined thickness of the preheat and reacton zone rather than just the thickness of the reaction zone was used in the residence time calculation because the heat required to evaporate particles can diffuse back into the preheat zone from the flame zone under these experimental conditions. Calculated values of residence time are listed in Table 3 as a function of composition, cold gas velocity, and flame temperature. The temperatures used in Equation 3-1 were the maximum flame temperature as measured at the end of the reaction zone; this selection of temperature is traditional.[25,35,39,59]

3.4 Laser Attenuation-Particle Evaporation Rate

The evaporation rates of particles of varying size were crudely measured using a laser attenuation method. From a plot of the magnitude of laser attenuation versus vertical distance above the burner surface, relative values of particle evaporation rate were deduced. For these experiments, however, the intensity of the laser line (2 milliwatts at 6328 Å) was too strong compared to the sensitivity of laser detection and the laser beam diameter is too wide compared to the required spatial resolution, so that only qualitative measurements

Table 3. Calculated values of particle residence time with varied
composition and cold gas velocity in methane/air flames.

Composition (∅)	Cold Gas Velocity (cm/sec)	Flame Temperature (°K)	Residence Time (milliseconds)
	10	1840	5.6
1.1	7	1770	8.3
	5	1720	11.9
	9	1750	6.5
0.9	7.5	1725	7.9
	5	1640	12.4

could be conducted. The incident laser intensity was attenuated
by the particles in the flames by only a small amount compared to
the original intensity of the signal. This attenuation remained
approximately constant from the preheat zone to post-flame zone,
independent of particle size range. This small degree of attenuation
seemed to be originating from the flame itself. With these findings
in mind, attenuation experiments using whole particles issuing through
the burner without the flame were conducted. It was found that
the incident laser intensity changed in a measurable way. These
experimental results are shown in Figure S. It was concluded that
all the particles were completely evaporated in the residence time
defined by the preheat zone plus reaction zone independent of par-
ticle size range. Furthermore, higher values of particle loading
were used in this experiment than those of the actual inhibition
experiment, so that all the particles were certainly evaporated in
these inhibited flames.

From Nusselt's shrinking droplet theory, the evaporation rate
of any solid particle can be approximately determined by the fol-
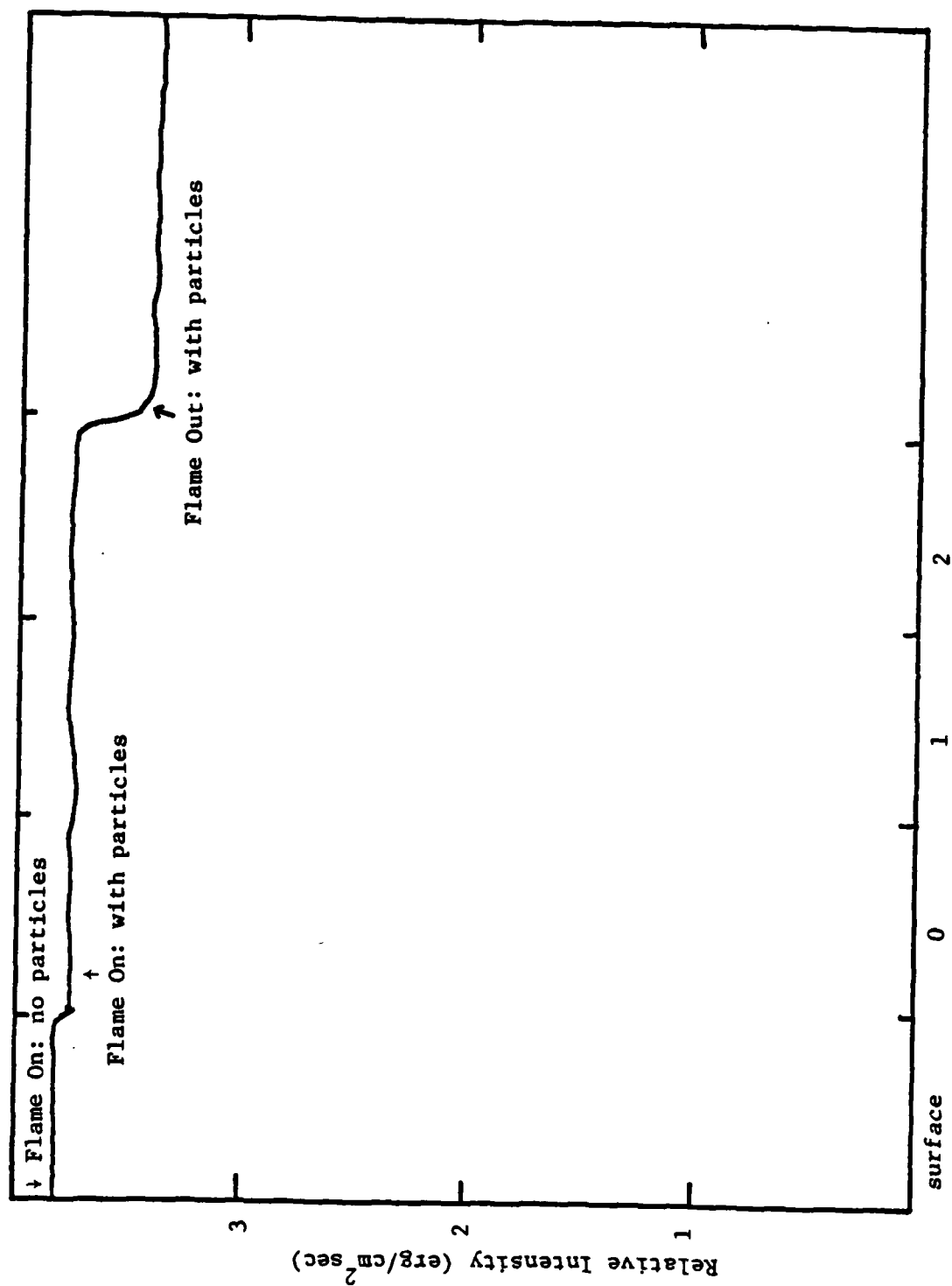lowing:[61]

$$\dot{W} = K_p \, W \, d^{-2} \qquad\qquad (3-2)$$

where: $\dot{W}$ = evaporation rate (g/sec)

K_p = evaporation constant (cm^2/sec)

W = weight of the particle (g)

d = diameter of the particle (cm).

Figure 8. Attenuated HeNe laser peak upon introduction of $NaHCO_3$ powders.

By manipulation of Equation 3-2, one can calculate the evaporation time of a particle:

$$t_{evp} = \frac{W}{\dot{W}} = \frac{d^2}{K_p} \qquad (3-3)$$

For all the ranges of particle size studied, the K_p value was held constant: only the representative diameter of the particles were changed. As a result, the evaporation time of a particle was proportional to the square of the mean particle diameter, i.e., bigger particles had a much longer evaporation time than smaller ones. Calculated values of evaporation time and evaporation rate are given in Table 4.

These calculated values appeared to contradict the experimental observation that all sized particles studied were completely evaporated at the end of the reaction zone. Such a contradiction can be explained by assuming a larger value of K_p, so that the evaporation time of the biggest particle is complete within the flame residence time.

The observation of complete particle evaporation in the flames is consistent with the predictions of Rosser, Inami, and Wise,[13] but disagrees with the conclusions drawn by DeWitte, Vrebosch, and Van Tiggelen.[21] It should be pointed out, however, that the experimental arrangement of this study maximized the opportunity for evaporation. The flame was rather a slow one, and the gases flowed in an upward direction. Thus, the particles were falling backward and may have spent an even longer time in the reaction zone than might otherwise be expected.[25]

Table 4. Calculated values of evaporation time and evaporation rate for one particle by Nusselt's droplet shrinking theory.

Particle Size Range (μ)	Representative Diameter, d (μ)	Initial Weight of 1 Particle, W (g)	Evaporation Rate, $\dot{W}$ (g/sec)	Evaporation Time, t (sec)
0-10	5	1.40×10^{-10}	$5.57 \times 10^{-4} K_p$	$2.50 \times 10^{-7}/K_p$
10-20	15	3.82×10^{-9}	$1.70 \times 10^{-3} K_p$	$2.25 \times 10^{-6}/K_p$
20-35	27.5	2.35×10^{-8}	$3.11 \times 10^{-3} K_p$	$7.56 \times 10^{-6}/K_p$

3.5 Temperature Rise Measurements Upon NaHCO$_3$ Flame Inhibition

Fuel-rich methane/air flames were used in temperature-rise experiments for the purpose of determining the effectiveness of inhibition powders. An attempt was made to obtain corresponding data in a fuel-lean flame at $\emptyset$ = 0.9, but for unknown reasons this mixture gave temperature rise values that were irreproducible and ambiguous.

It has been shown that a valid measure of inhibition of a quenched premixed flame burning at a constant unburned gas velocity is a rise in temperature in the inhibited flame, relative to the uninhibited flame.[62] This phenomenon can be understood as follows. When a quenched flame burning at constant velocity is inhibited, some one or more critical reactions are impeded. This causes the flame to burn less closely to the burner, or lift it off slightly, thus reducing the temperature gradient and heat transfer back to the burner surface. As a result, the gas temperatures throughout the flame increase so that presumably the rates of the critical reactions, previously slowed by the inhibitor, increase to the point where they can continue to consume the constant throughput of fuel and air. The net reduction in heat transfer then shows up as a temperature rise in the burned gas.

Most workers who have considered the possibility of homogeneous inhibition have postulated that it takes place through sodium-atom-catalyzed-radical recombination.[13,14,63] Thus, plots of temperature rise against sodium atom concentration are useful. Those obtained in this study are shown in Figure 9, as a function of varying particle
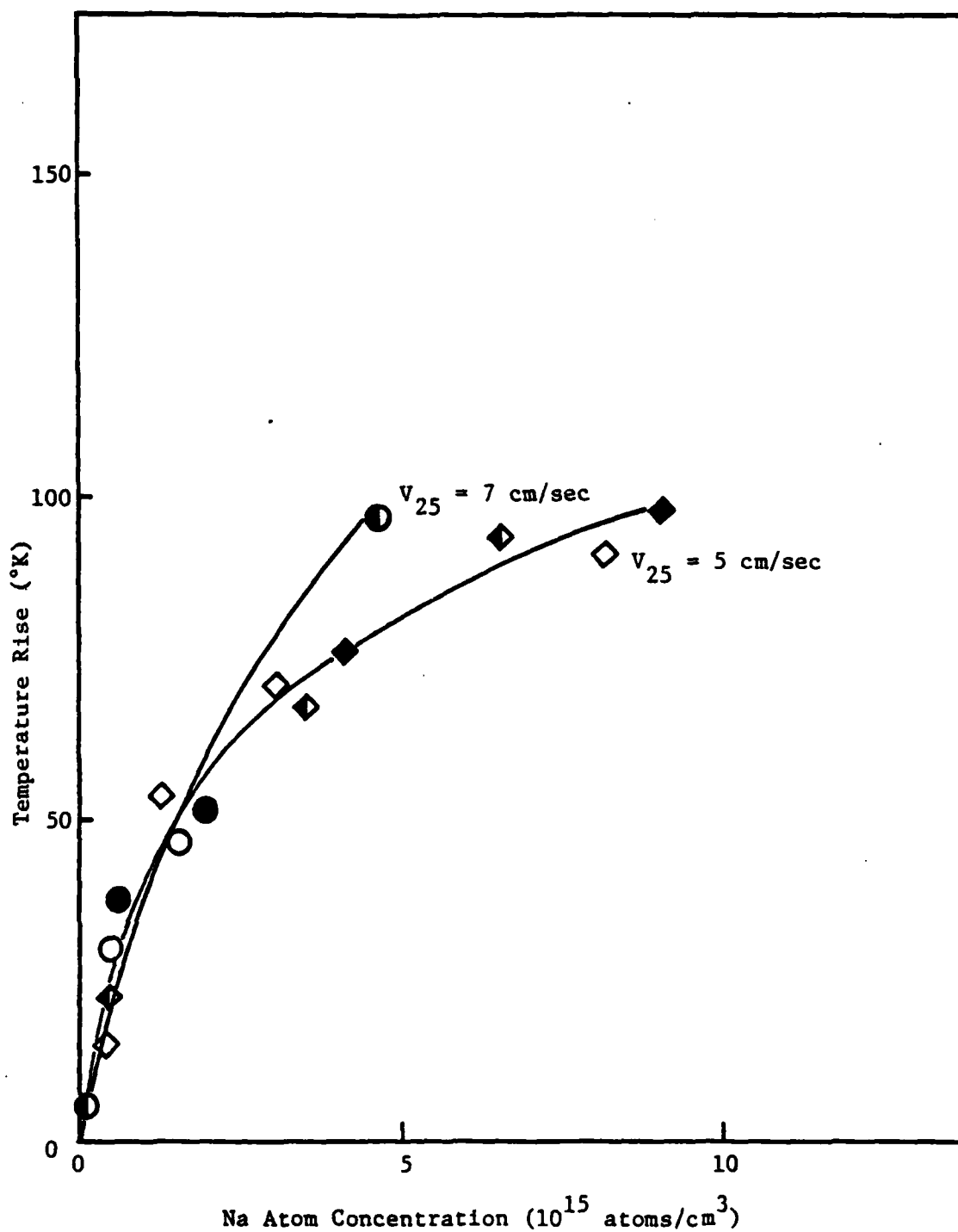
Figure 9. Sodium atom concentration versus the temperature rise
upon inhibition as a function of particle size (closed
symbols: 0-10 microns; half-closed symbols: 10-20 microns;
open symbols: 20-35 microns) in $\emptyset$ = 1.1 methane/air flames.

size. Sodium atom concentrations in Figure 9 were represented by the unit of atoms/cm^3, which was calculated:

$$[Na] = \frac{\dot{m}}{\dot{V}} \frac{T_f}{T_o} \times \frac{6.023 \times 10^{23}}{MW} \tag{3-4}$$

where [Na] = sodium atom concentration (atoms/cm^3)

    $\dot{m}$ = rate of weight loss (g/sec)

    $\dot{V}$ = volume flow rate (cm^3/sec)

    MW = molecular weight of NaHCO$_3$ (g/mol).

Flames with the same composition but a faster cold gas velocity (V_{25} = 10 cm/sec) did not show any temperature rise upon introduction by the same inhibitor powders, independent of particle size. From the calculations of particle residence time given in Table 3, these flames provide a residence time of 5.6 milliseconds. This small value of residence time may not be enough to commence the decomposition of the inhibitor powders in the reaction zone so that they had no effectiveness.

In contrast to the residence time effect on the evaporation mechanism of powders, Figure 9 shows that the inhibiting action of powders has a temperature dependence as well. Flames whose cold gas velocity is 5 cm/sec have longer residence times than flames whose cold gas velocity is 7 cm/sec. Flames with a lower cold gas velocity are expected to be more inhibited than those with a higher cold gas velocity from a residence time viewpoint. This reasoning is contradicted by the experimental results shown in Figure 9. With these findings in mind, it was concluded that the time-temperature

history of the inhibitor powder was important in determining the inhibition effectiveness.

The effect of particle size on the inhibition action was also investigated; these results are also included in Figure 9. All the measurements lie on the same lines, independent of particle size within the experimental error. This result is in good agreement with the laser attenuation measurements, which also demonstrated that all the differently-sized powders were apparently evaporated within the time-temperature limitation of the flame, independent of particle size.

3.6 Species Concentration Measurements Upon $NaHCO_3$ Inhibition

Concentrations of major species (CH_4, CO, CO_2, O_2, H_2O) were determined by gas chromatography as a function of sodium atom concentration. All the concentration measurements were conducted on flames whose composition was fuel-rich ($\emptyset$ = 1.1), and with added particles of different sizes. Flames having a cold gas velocity of cm/sec showed no dramatic change in their species concentration after $NaHCO_3$-doping as is illustrated in Figure 10. This finding is in good agreement with the fact that no temperature rise was witnessed upon addition of $NaHCO_3$. The amount of change in species concentration matched well to the amount of change in temperature rise. Apparently the residence time was too short to evaporate powders in methane/air flames (V_{25} = 10 cm/sec) even though their temperature was high. Flames with a lower cold gas velocity (V_{25} = 7 or 5 cm/sec) had lower flame temperatures but longer residence times, and changed more dramatically in species concentration as well as
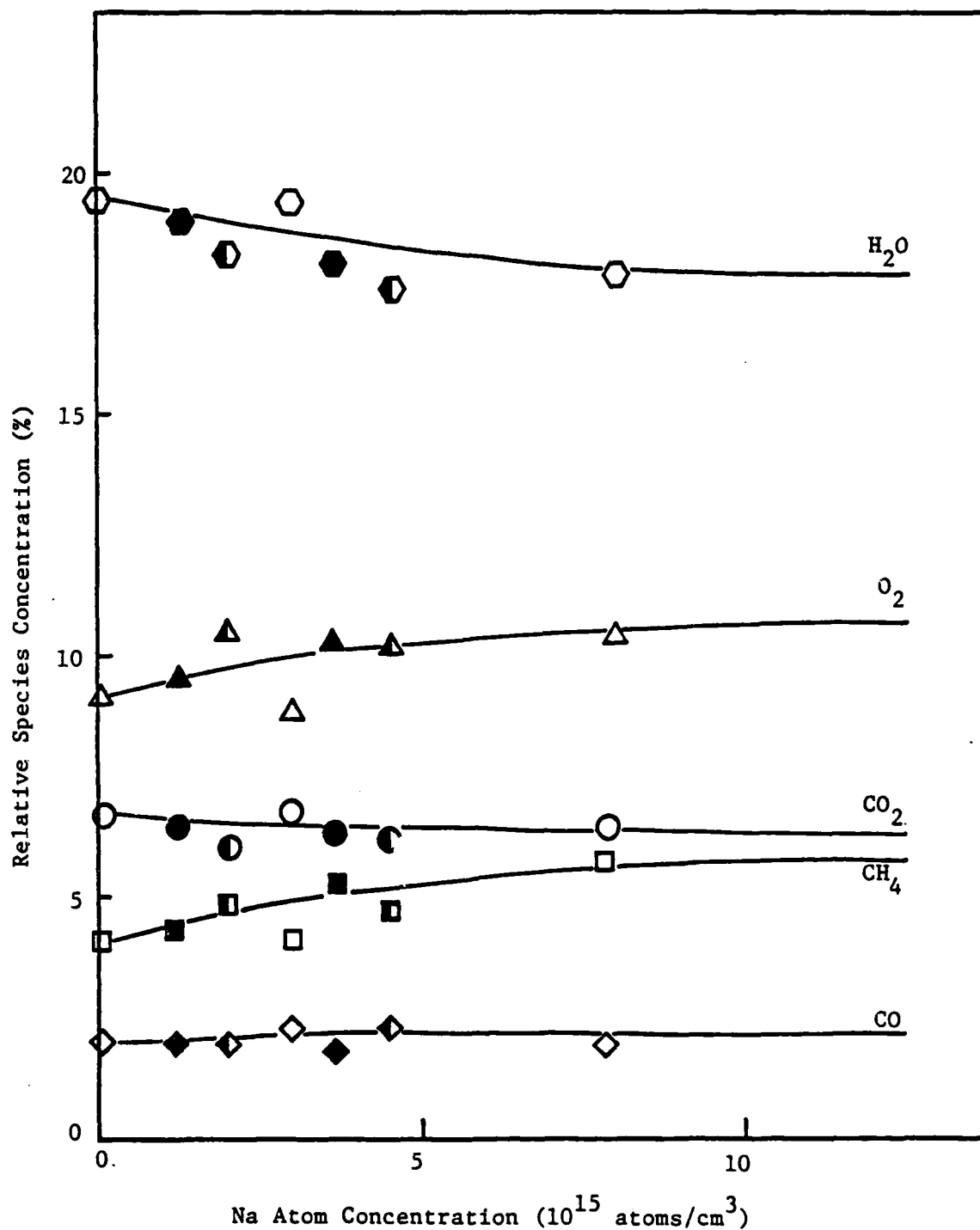
Figure 10. Sodium atom concentration versus products of combustion species concentration upon inhibition as a function of particle size (closed symbols: 0-10 microns; half-closed symbols: 10-20 microns; open symbols: 20-35 microns) in a ϕ = 1.1 methane/air flame at V_{25} = 10 cm/sec.

temperature upon inhibition. No particle size effect was observed in Figures 10, 11, and 12, as is illustrated by the fact that all the data points fell on one line independent of particle size.

Upon introduction of inhibitor powder, it had been expected by many researchers that major products (CO_2, H_2O) would decrease, and that combustion intermediates (CO, H_2) and reactants (CH_4, H_2) would increase.[65,66] Figures 10, 11, and 12 show that the experimental results obtained in this program were in good agreement with these expectations.

Most workers have postulated that a homogeneous inhibition mechanism takes place via sodium-atom-catalyzed-radical-recombination reactions, such as:[13,14,25,63]

$$Na + R + M = NaR + M \qquad [3\text{-}1]$$

$$NaR + R´ = Na + RR´ \qquad [3\text{-}2]$$

where: R or R´ = H, O, or OH radical

M = third body.

In addition, another reaction pathway of sodium has been postulated:

$$Na + O_2 + M = NaO_2 + M \qquad [3\text{-}3]$$

Formation of NaO_2 in Reaction [3-3] is followed by:

$$NaO_2 + R = NaR + O_2 \qquad [3\text{-}4]$$

This NaR inhibits the flame by removing radicals through the path of Reaction 3-2. However, a glance at Reactions 3-1 and 3-2 shows that this line of attack is untenable. Reaction 3-3 and presumably

Figure 11. Sodium atom concentration versus products of combustion species concentration upon inhibition as a function of particle size (closed symbols; 0-10 microns; half-closed symbols: 10-20 microns; open symbols: 20-35 microns) in a $\emptyset$ = 1.1 methane/air flame at V_{25} = 7 cm/sec.
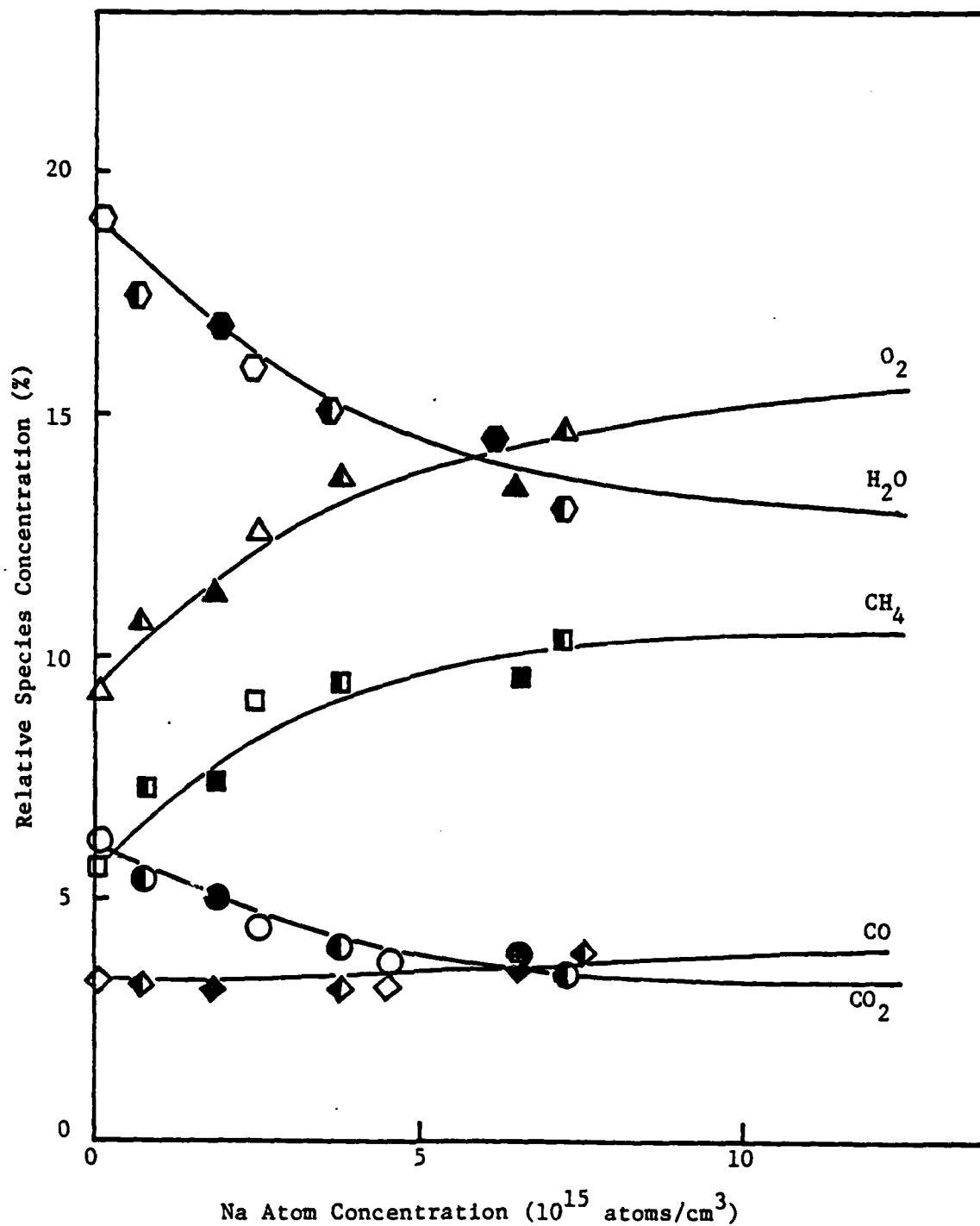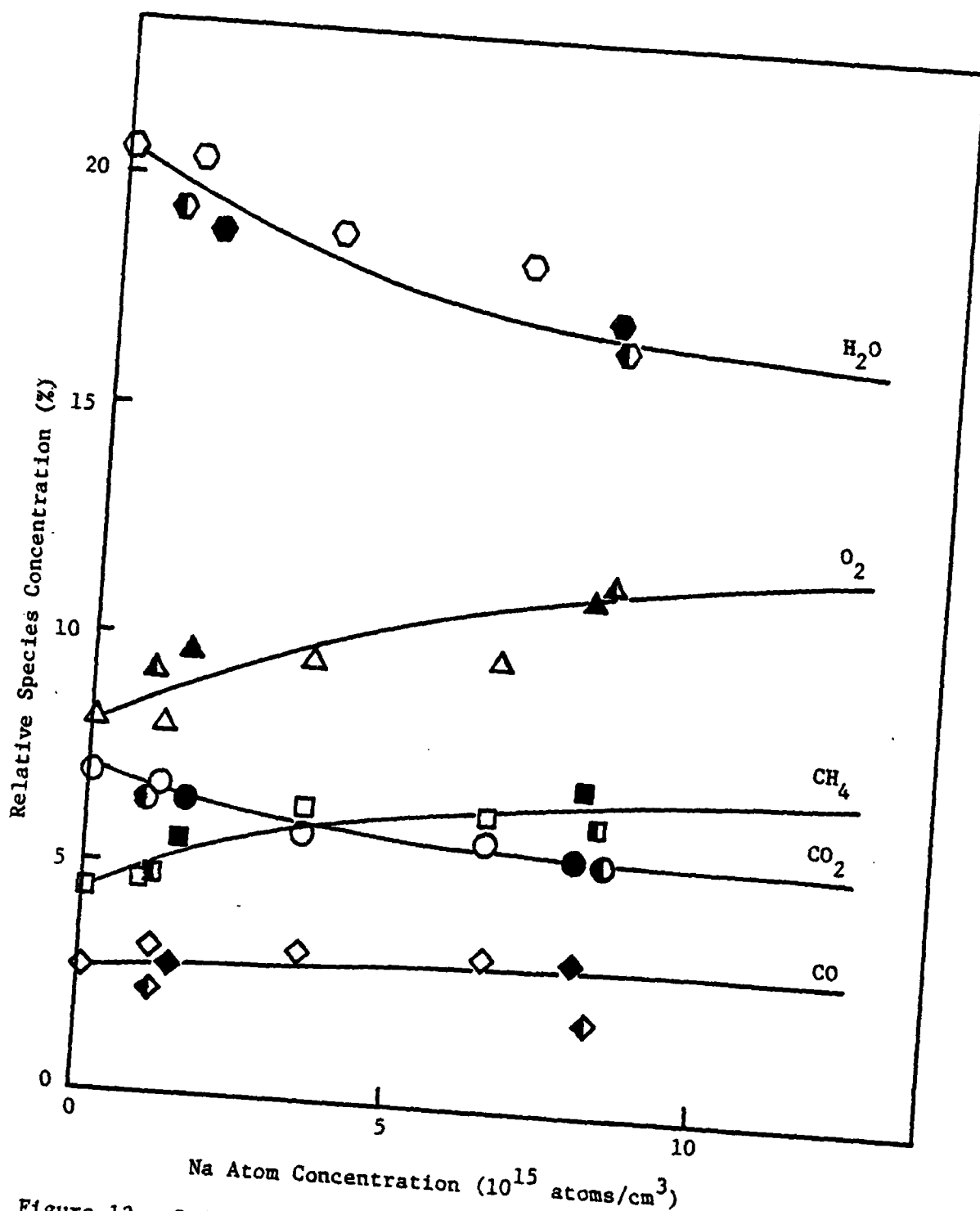
Figure 12. Sodium atom concentration versus products of combustion species concentration upon inhibition as a function of particle size (closed symbols: 0-10 microns; half-closed symbols: 10-20 microns; open symbols: 20-35 microns) in a $\emptyset = 1.1$ methane/air flame at $V_{25} = 5$ cm/sec.

those represented by Reaction 3-1 are efficient three-body recombination reactions. As a result, in order for sodium atoms to contribute to the recombination of the radical pool, the sodium atom concentration should be of the same order of magnitude as radical concentrations. With these findings in mind, Iya, et al.,[25] investigated the catalytic effect of sodium atoms in recombination of radicals. They concluded from their calculation of OH concentration and the rate constants of Reaction 3-1 that: (1) the idea that inhibition does, in fact, arise from competing inhibitor-catalyzed radical recombination is a tenable one; and (2) the problem lies in explaining how Na atoms can be so efficient.

Unusually large catalytic efficiencies of metals in flames are known, as a number of examples have been presented by Bulewicz and Padley.[66] These authors did not employ such high sodium atom concentrations as were used here. They suggested as a general mechanism the formation of excited states between Na and R in a two-body reaction followed by the equivalent of Reaction 3-2.

As an alternative to the aforementioned reasoning, Iya, et al.,[25] suggested a bound complex between H_2O and Na, stabilized by a dipole-induced interaction. The H_2O, which is present in large amounts in methane/air flames and is so throughout the entire experimental range of sodium atom concentration, as is shown in Figures 10, 11, and 12 has a large dipole moment. The alkalies, on the other hand, are highly polarizable because of their single outer shell electrons. Thus, on the approach of an alkali, A, to a water molecule, there will be a dipole induced in A. Postulation

was made that the result would be a loosely-bound $A \cdot H_2O$ molecule with sufficient stability to be kinetically significant. Then, the inhibition mechanism by sodium atoms would be the following:

$$Na + H_2O + M = Na \cdot H_2O + M \qquad [3-5]$$

$$Na \cdot H_2O + R = NaR + H_2O \qquad [3-6]$$
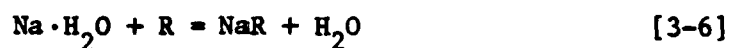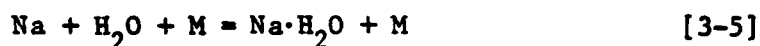
NaR in Reaction 3-6 then would react as in Reactions 3-2. This concept of the sodium-atom inhibition mechanism does two things. First, the slow Reaction 3-1 is replaced with a faster one (Reaction 3-5), because the water concentration is much greater than the radical concentration. Secondly, it explains why potassium and the heavier alkalies are more effective than sodium, as they are more polarizable.

3.7 Inhibition Index of NaHCO_3

A measure of inhibition applicable to quenched premixed flat flames was introduced by Iya, et al.[62] They found that for constant-velocity quenched flames, inhibition was characterized by a rise in maximum flame temperature. The numerical index for evaluating the effectiveness of inhibitors in quenched flames is given by:[67]

$$I_T^Q = \frac{T_i^{MAX} - T_o^{MAX}}{[I]} \qquad (3-5)$$

where I_T^Q = inhibition index for quenched flame

T_i^{MAX} = inhibited flame maximum temperature

T_o^{MAX} = clean flame maximum temperature

[I] = inhibitor mole fraction.

Calculated values of inhibitor indices of various inhibitors are reported in Table 5. This new measure of inhibition has been used to demonstrate gas phase inhibition by CH_3Br[68] and CF_3Br[55] and to examine the concept of self-inhibition.[35] All the experimental results showed that this new measure of inhibition was well correlated with the burning-velocity-reduction criterion for inhibition of adiabatic flames.

To better understand the inhibition mechanism of $NaHCO_3$ powder, inhibition indices were calculated as a function of clean maximum flame temperature (1720, 1725, 1750, 1770°K). For each flame of these temperatures, inhibition indices were calculated and are listed in Table 6. Based on the values in Table 6, Figure 13 is drawn to illustrate a plot of sodium atom concentration versus temperature rise upon inhibition. Figure 13 shows that the higher the base-line temperature, the more effective a given powder is to inhibit the flame. From this fact it is concluded that temperature is important in the evaporative action of powders.

Researchers at the U.S. Bureau of Mines found, by actually detonating a mine gallery, that $NaHCO_3$ was ineffective at stopping a coal mine dust explosion that had a flame temperature of 1500 ± 50°K.[9] They suspected that this flame temperature may not have been high enough for the $NaHCO_3$ to become "chemically activated,"

Table 5. Measures of inhibitor effectiveness for selected agents.

Inhibitor	I_T^Q	I_V^A
H_2O (liquid)	–	0.6
CO_2 (gaseous)	–	0.9
CH_3Br (gaseous)	225	13
$NaHCO_3$ (solid)	3000*	160

I_T^Q = inhibitor effectiveness measured by temperature rise on a quenched flame (°K)

I_V^A = inhibitor effectiveness measured by burning velocity decrease of an adiabatic flame[11,67] (dimensionless)

*Datum determined for the first time by this study

Table 6. Inhibition index of $NaHCO_3$ in methane/air flame with varied composition and cold gas velocity.

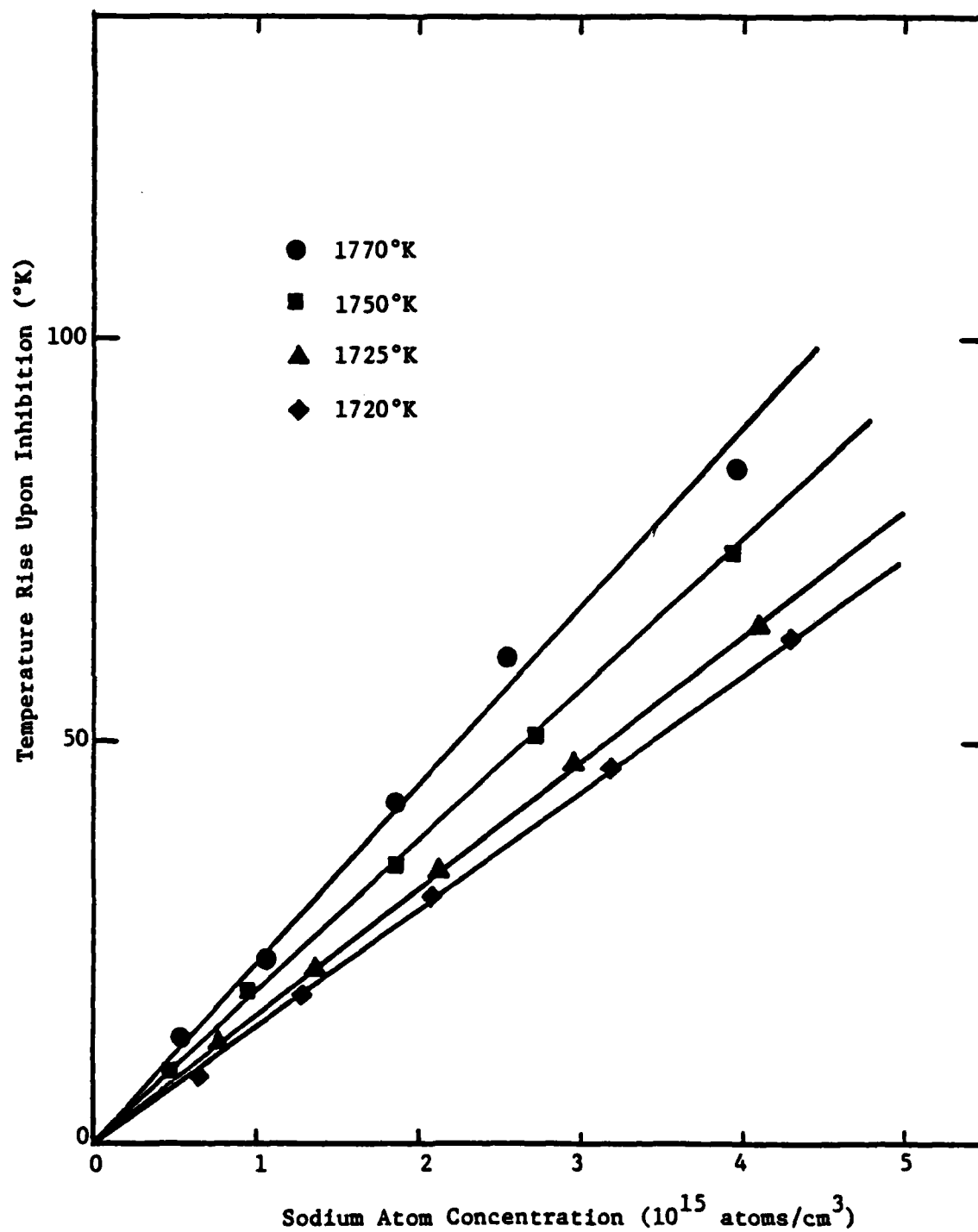| Stoichiometry (∅)	Cold Gas Velocity (cm/sec)	Flame Temperature (°K)	Inhibition Index
1.1	7	1770	3880
1.1	5	1720	2680
0.9	9	1750	3140
0.9	7.5	1725	2800

Figure 13. Sodium atom concentration versus the temperature rise upon inhibition as a function of flame temperature in methane/air flames.

i.e., decomposed. With this in mind, a plot of flame temperature against inhibitor effectiveness is presented in Figure 14. Extrapolation of these inhibition effectiveness data to zero yields the flame temperature at which $NaHCO_3$ agent would be completely ineffective at suppressing combustion, ca., 1650°K. This lower temperature limit is in line with that actually determined under explosive conditions by researchers of U.S. Bureau of Mines.[9] Furthermore, experiments were carried out here on a 1640°K flame and showed that $NaHCO_3$ powder had no inhibitor effectiveness. A flame whose maximum temperature was 1640°K had a long enough residence time to evaporate powders (see Table 3). From these findings, it was concluded that temperature is a major factor in decomposition of inhibitor powders in flame. To be sure, temperature along with time is a significant parameter in determining the effectiveness of inhibitor powders.
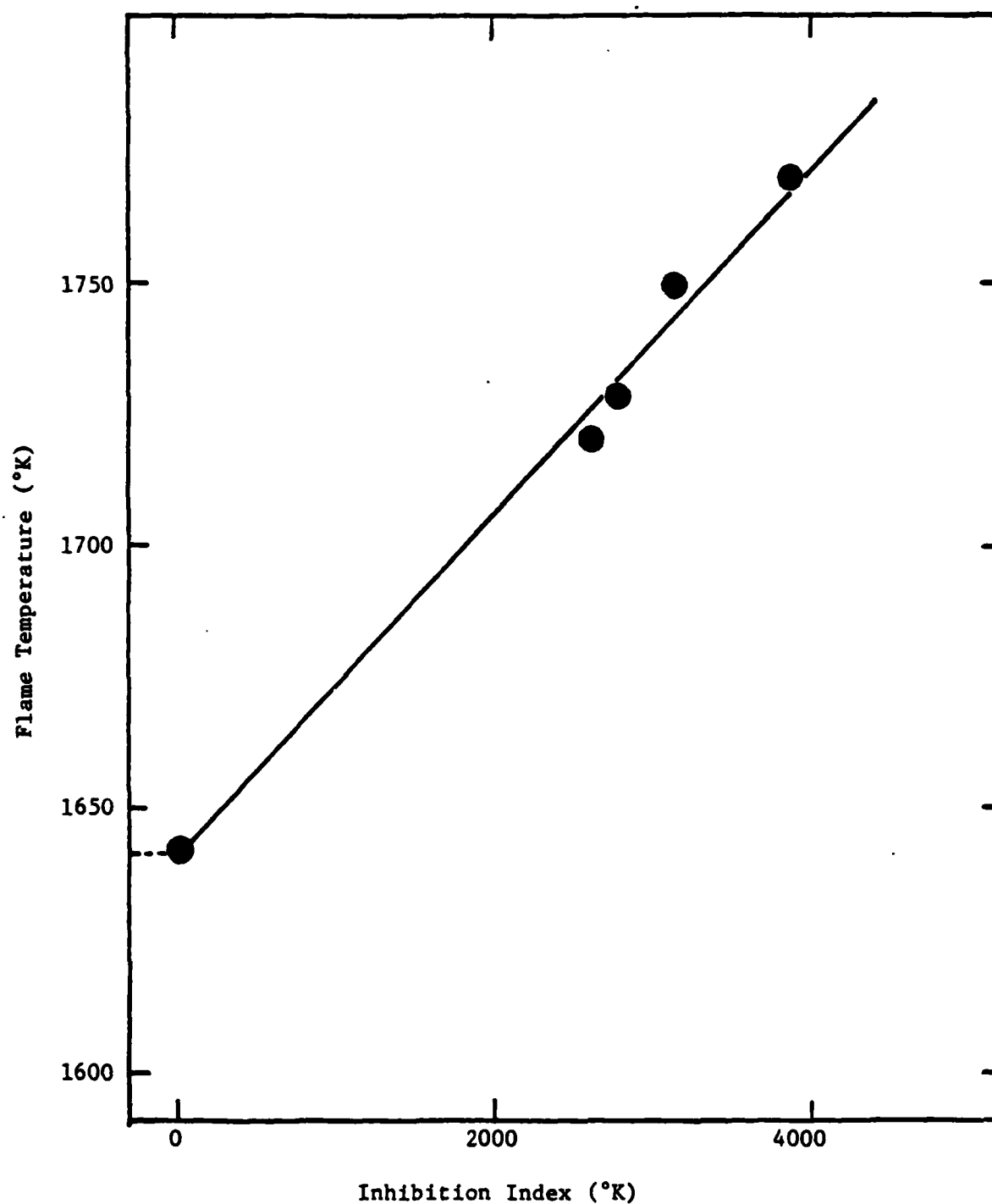
Figure 14. NaHCO₃ inhibitor effectiveness in $\emptyset$ = 1.1 methane/air flames as a function of flame temperature.

CHAPTER 4

CONCLUSIONS

The ability of $NaHCO_3$ powders to inhibit methane/air flames with varied compositions and temperatures has been evaluated. The dependence of this effectiveness of inhibition as a function of sodium atom concentration has been measured. A good correlation has been found between the concentration of sodium atoms produced by sodium bicarbonate powders of various particle sizes and the degree of inhibition. This correlation is independent of the diameter of the particle over the range studied. This finding provides strong evidence that the $NaHCO_3$ inhibition mechanism is homogeneous in nature. The residence time of a particle in the flame zone at the flame temperature has also been determined for various compositions and cold gas velocities. Limiting values of residence time and temperature on effectiveness were determined. These findings support the concept that the time-temperature history of sodium atoms in flames is critically important in the homogeneous suppression mechanism. Indeed, extrapolation of these singular inhibitor effectiveness data to zero yields the maximum flame temperature at which $NaHCO_3$ would be expected to be completely ineffective at suppressing unwanted combustion, ca. 1600°K. This type of information should be of great value to fire-fighters, because it helps them to identify which agent would be most effective (or not effective at all), depending upon the nature of the fire.

CHAPTER 5

SUGGESTIONS FOR FURTHER RESEARCH

1. Because of experimental design limitations, which may in fact be specified by natural flame propagation, no flames of $\emptyset$ outside of ± 20% stoichiometric were probed in this study. In real fires, flame compositions can vary considerably, so that further inhibition research on more fuel-lean and more fuel-rich flames is needed for a better simulation of practical fire events. Novel burners will be required for this to be done.

2. By extrapolation, it was learned that $NaHCO_3$ powders were ineffective as inhibitors at temperatures below 1600°K. Experiments at lower temperatures are needed for the validation of this finding.

3. Quantitative laser attenuation measurements are required for more accurate evaporation time determinations. It was concluded that the present laboratory equipment could only qualitatively measure evaporation rates because of rather poor spatial resolution and inadequate light detection. A differently specified apparatus is required for experimental results on the time-temperature history on particles to be better defined.

4. Concentrations of transient species, such as OH, H, and O, are important in the understanding of flame suppression mechanisms. Because combustion reactions are propagated with the aid of these transient species, concentration measurements on OH, H, and O are necessary to enable one to learn more about the inhibition mechanism of dry chemicals.

5. Salts other than $NaHCO_3$ should be studied, with dispatch, for the determination of their effectiveness. Experiments on hybrid mixtures of salts and water should also be conducted because of the probability of synergistic effects for these combined flame suppressants.

REFERENCES

1. Essenhigh, R.: "Discussion of Dust Explosions," Mineral In-
   dustries Experiment Station Circular No. 64, The Pennsylvania
   State University, 1963.

2. Grumer, J.: "Recent Research Concerning Extinguishment of
   Coal Dust Explosions," Fifteenth Symposium (International)
   on Combustion, p. 103, The Combustion Institute, 1975.

3. Richmond, J., Liebman, I., Bruszak, A., and Miller, J.: "A
   Physical Description of Coal Mine Explosions. Part II,"
   Seventeenth Symposium (International) on Combustion, p. 1257,
   The Combustion Institute, 1979.

4. Office of Technology Assignment, Congress of the United States,
   Washington, D.C., 1979. "The Direct Use of Coal, Prospects
   and Problems of Production and Combustion."

5. Sapko, M., Furno, A., and Kuchta, J.: "Quenching Methane-
   Air Ignitions with Water Sprays," U.S. Bureau of Mines Report
   of Investigations RI 8214, 1977.

6. Liebman, I., Corry, J., Pro, R., and Richmond, J.: "Extin-
   guishing Agents for Mine Face Gas Explosions," U.S. Bureau
   of Mines Report of Investigations RI 8294, 1978.

7. Burgess, D., Hertzberg, M., Richmond, J., Liebman, I., Cash-
   dollar, K., and Lazzara, C.: "Combustion, Extinguishment,
   and Devolatilization in Coal Dust Explosions," Paper 79-13,
   Western States Section Combustion Institute Spring Technical
   Meeting, Provo, UT, April 1979.

8. Liebman, I., Richmond, J., and Grumer, J.: "Recent Develop-
   ments in Passive and Triggered Explosion Barriers," Paper VII
   4.1, Sixteenth International Conference on Coal Mine Safety
   Research, Washington, D.C., September 1975.

9. Burgess, D.: "Recent Studies of Coal Dust Explosions," Paper
   27, Eastern States Section Combustion Institute Fall Technical
   Meeting, FL, November 1978.

10. Friedman, R. and Levy, J.: "Survey of Fundamental Knowledge
    of Mechanisms of Action of Flame Extinguishing Agents," Wright
    Air Development Center Technical Report 56-568, January 1957;
    Supplement I, September 1958; Supplement II, April 1959.

11. Reuther, J.: "Comments on Chemical and Physical Inhibition
    of Quenched and Adiabatic Premixed Flames," Paper IV-31,
    Eastern States Combustion Institute Fall Technical Meeting,
    East Hartford, CT, November 1977.

12. Hastie, J.: "Molecular Basis of Flame Inhibition," J. Research Natl. Bur. Standards 77A, 733 (1973).

13. Rosser, W., Inami, S., and Wise, H.: "The Effect of Metal Salts on Premixed Hydrocarbon-Air Flames," Combustion and Flame 7, 107 (1963).

14. Friedman, R. and Levy, J.: "Inhibition of Opposed-Jet Methane-Air Diffusion Flames. The Effects of Alkali Metal Vapors and Organic Halides," Combustion and Flame 7, 195 (1963).

15. Lafitte, P., Delbourgo, R., Comburieu, J., and Dumont, J.: "The Influence of Particle Diameter on the Specificity of Fine Powders in the Extinction of Flames," Combustion and Flame 9, 357 (1965).

16. Birchall, J.: "On the Mechanism of Flame Inhibition by Alkali Metal Salts," Combustion and Flame 14, 85 (1970).

17. Dodding, R., Simmon, R., and Stephens, A.: "The Extinction of CH_4-Air Diffusion Flames by Sodium Bicarbonate Powders," Combustion and Flame 15, 313 (1970).

18. Dolan, J. and Dempster, P.: "The Suppression of Methane-Air Ignitions by Fine Powders," J. Appl. Chem. Lond. 5, 510 (1955).

19. Dolan, J.: "The Suppression of CH_4/Air Ignitions by Fine Powders," Sixth Symposium (International) on Combustion, p. 787, Reinhold, 1957.

20. Lee, T. and Robertson, A.: "Effectiveness of Some Powdered Materials in Extinguishing Hydrocarbon Fires," International Symposium on the Use of Models in Fire Research, Natl. Acad. of Science, Publ. No. 786, p. 93 (1961).

21. DeWitte, M., Vrebosch, J., and van Tiggelen, A.: "Inhibition and Extinction of Premixed Flames by Dust Particles," Combustion and Flame 8, 257 (1964).

22. Ksandapulo, G., Kolesnikov, B., Zavadsky, V., Odnorog, D., and Elovskaya, T.: "Inhibition Mechanism of Combustion of Hydrocarbon-Air Mixtures by Finely Dispersed Particles," Fiz. Goreniya Vzryva 7, 92 (1971).

23. Wise, H. and Rosser, W.: "Homogeneous and Heterogeneous Reactions of Flame Intermediates," Ninth Symposium (International) on Combustion, p. 733, Academic Press, 1963.

24. Hoffman, W.: "Influence on the Laminar Flame Velocity with Alkali Metal Salts," Chem. Ing. Techn. 43, 556 (1971).

25. Iya, K., Wollowitz, S., and Kaskan, W.: "The Mechanism of Flame Inhibition by Sodium Salts," Fifteenth Symposium (International) on Combustion, p. 329, The Combustion Institute, 1975.

26. McHale, E.: "Flame Inhibition by Potassium Compds," Combustion and Flame 24, 277 (1975).

27. Woolhouse, R. and Sayers, D.: "Monnex Compared with Other Potassium Based Dry Chemicals," Fire Journal 67, 85 (1973).

28. Altman, R.: "Laboratory Evaluation of Dry Chemical Fire Extinguishants," Western States Section Combustion Institute Fall Technical Meeting, El Segundo, CA, October 1973.

29. Grumer, J. and Bruszak, A.: "Inhibition of Coal Dust-Air Flames," U.S. Bureau of Mines Report of Investigations 7552, 1971.

30. Milne, T. and Beachy, J.: "The Microstructure of Pulverized Coal-Dust Flames. II. Gaseous Species, Particulate, and Temperature Profiles," Combustion Sci. and Tech. 16, 139 (1977).

31. Smoot, L. and Horton, M.: "Exploratory Studies of Flame and Explosion Quenching," U.S. Bureau of Mines Final Report No. GO 177034, March 1978.

32. Cashdollar, K. and Hertzberg, M.: "Measurements of Particle and Gas Temperatures of Coal Dust Explosions and Flames," Paper 29, Eastern States Section Combustion Institute Fall Technical Meeting, Miami, FL, November 1978.

33. Haynes, W., Gasior, S. and Forney, A.: "Catalysis of Coal Gasification at Elevated Pressure," p. 179, Coal Gasification, Advances in Chemistry Series 131, L. Massey, Ed. (A.C.S., Washington, D.C., 1974).

34. Kaskan, W.: "The Dependence of Flame Temperature on Mass Burning Velocity," Sixth Symposium (International) on Combustion, p. 134, Reinhold, 1957.

35. Kaskan, W. and Reuther, J.: "Limiting Equivalence Ratio, Dissociation, and Self-Inhibition in Premixed, Quenched, Fuel-Rich Hydrocarbon/Air Flames," Sixteenth Symposium (International) on Combustion, p. 1083, The Combustion Institute, 1977.

36. Anderson, J. and Friedman, R.: "An Accurate Gas Metering System for Laminar Flow Studies," Rev. Sci. Instr. 20, 61 (1949).

37. Strauss, W. and Edse, R.: "Vacuum-Type Gas-Flow Calibrator," Rev. Sci. Instr. 30, 258 (1959).

38. Kydd, P.: "The Extended Range Critical Flow Orifice Meter and Its Application," General Electric Research Laboratory Memo Report, No. C-61-46, March 1961.

39. Fristrom, R. and Westenberg, A.: Flame Structure, McGraw-Hill, N.Y., 1965.

40. Friedman, R.: "Measurement of the Temperature Profile in a Laminar Flame," Fourth Symposium (International) on Combustion, p. 274, Williams and Wilkins, 1953.

41. Leah, A. and Carpenter, N.: "The Estimation of Atomic Oxygen in Open Flames and the Measurement of Temperature," Fourth Symposium (International) on Combustion, p. 274, Williams and Wilkins, 1953.

42. Gaydon, A. and Wolfhard, H.: Flames, Their Structure, Radiation, and Temperature, Third ed., Chapman and Hall, London, 1970.

43. McAdams, W.: Heat Transmission, 3rd ed., McGraw-Hill, N.Y., 1954.

44. U.S. Department of Commerce, National Bureau of Standards, Circular 564, Washington, D.C., 1955. "Tables of Thermal Properties of Gases."

45. Biordi, J., Lazarra, C., and Papp, J.: "Chemical Flame Inhibition Using Molecular Beam Mass Spectroscopy Buromotrifluomethane in Low-Pressure CH_4-O_2-Ar Flames," U.S. Bureau of Mines Report of Investigation No. 7723, 1974.

46. Harmor, R. and Smith, I.: "Fluidizing Feeders for Providing Fine Particles at Low, Stable Flows," Fuel 50, 394 (1971).

47. Hardesty, R., Pohl, J., and Stark, A.: "The Rates and Mechanisms of Pulverized Coal Combustion-First Annual Report," SAND 78-8234, 1978.

48. Coulson, J. and Richardson, J.: Chemical Engineering, Vol. 2, Pergamon Press, N.Y., 1962.

49. Kunii, D. and Levenspiel, O.: Fluidization Engineering, John Wiley and Sons, Inc., N.Y., 1962.

50. Wen, C. and Simons, H.: "Flow Characteristics in Horizontal Fluidized Solids Transport," A.I.Ch.E. Journal 5, 263 (1959).

51. Fristrom, R., Prescott, R., and Grunfelder, C.: "Flame Zone Studies III-Techniques for the Determination of Composition Profiles of Flame Front," Combustion and Flame 1, 102 (1957).

52. Porter, R., Clark, A., Kaskan, W., and Browne, W.: "A Study of Hydrocarbon Flames," Eleventh Symposium (International) on Combustion, p. 907, The Combustion Institute, 1967.

53. Smith, S., and Gordon, A.,: "Precombustion Reactions in Hydrocarbon Diffusion Flames: The Praffin Candle Flame," J. Chem. Phys. 22, 1150 (1954).

54. Tine, G.: Gas Sampling and Chemical Analysis in Combustion Processes, Pergamon Press, N.Y., 1961.

55. Biordi, J., Lazarra, C., and Papp, J.: "On the Inhibition of Low Pressure Quenched Flames by CH_3Br," Combustion and Flame 23, 73 (1974).

56. Friedman, R., and Cyphers, S.: "Flame Structure Studies III, Gas Sampling in a Low-Pressure Propane-Air Flame," J. Chem. Phys. 23, 1875 (1955).

57. Willard, H., Merritt, L., and Dean, J.: Instrumental Methods of Analysis, D. Van Nostrand Company, N.Y., 1974.

58. Wersborg, B., Fox, L., and Howard, J.: "Soot Concentration and Adsorption Coefficient in a Low-Pressure Flame," Combustion and Flame 24, 1 (1975).

59. Glassman, I.: Combustion, Academic Press, Inc., N.Y., 1977.

60. Lewis, B. and von Elbe, G.: Combustion, Flames and Explosion of Gases, Academic Press, Inc., N.Y., 1961.

61. Kanury, M.: Introduction to Combustion Phenomena, Gordon and Breach, Science Publishers, Inc. N.Y., 1975.

62. Iya, K., Wollowitz, S. and Kaskan, W.: "The Measure of the Inhibition of Quenched Premixed Flames," Combustion and Flame 22, 415 (1974).

63. Creitz, E.: "Survey of the Chemistry of Flame Inhibition," J. Research Natl. Bur. Standards 74A, No. 4 (1970).

64. Fristrom, R. and Sawyer, R.: "Flame Inhibition Chemistry," Paper Presented at the Thirty-seventh AGARD Symposium on Aircraft, Fuels, Lubricants, and Fire Safety, The Hague, Netherlands, 1971.

65. Fenimore, C.: Chemistry of Pre-Mixed Flames, Pergamon Press, N.Y., 1964.

66. Bulewicz, E. and Padley, P.: "Catalytic Effect of Metal Additives on Free Radical Recombination Rates in $H_2 + O_2 + N_2$ Flames," Thirteenth Symposium (International) on Combustion, The Combustion Institute, p. 73, 1971.

67. Reuther, J.: "Measures of Effectiveness and Mechanisms for Chemical and Physical Inhibition of Quenched and Adiabatic Premixed Flames," Characterization of High Temperature Vapors and Gases, Vol. 2:1281-1313 NBS Special Publication 561: Proceedings of the 10th Materials Research Symposium, J. Hastie (Ed.), NBS (1979).

68. Hayes, K. and Kaskan, W.: "Inhibition of CH_3Br of CH_4/Air Flames Stabilized on a Porous Burner," Combustion and Flame 24, 405 (1975).

DISTRIBUTION LIST FOR TM 82-235

Commander (NSEA 0342)
Naval Sea Systems Command
Department of the Navy
Washington, DC 20362   Copies 1 and 2

Commander (NSEA 9961)
Naval Sea Systems Command
Department of the Navy
Washington, DC 20362   Copies 3 and 4

Defense Technical Information Center
5010 Duke Street
Cameron Station
Alexandria, VA 22314   Copies 5 through 10

END

FILMED

3-83

DTIC